

AD/A-006 403

SYNERGISTIC AND NOVEL EFFECTS IN
COMPOSITE SOLID PROPELLANT COMBUSTION

Warren C. Strahle, et al

Georgia Institute of Technology

Prepared for:

Office of Naval Research

1 October 1974

DISTRIBUTED BY:

NTIS

National Technical Information Service
U. S. DEPARTMENT OF COMMERCE

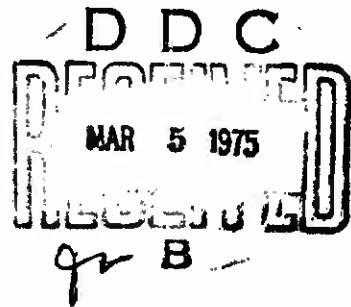
078080

**SYNERGISTIC AND NOVEL EFFECTS
IN COMPOSITE SOLID PROPELLANT COMBUSTION**

W. C. Strahle

J. C. Handley

October 1, 1974



**Second Annual Summary Report - Research Spansared
by
The Office of Naval Research**

**ONR Contract Na. N0014-67-A-0159-0016 ✓
Requisition Purchase Request NR 092-543**

Reproduced by
**NATIONAL TECHNICAL
INFORMATION SERVICE**
US Department of Commerce
Springfield, VA. 22151

Approved for Public Release; Distribution Unlimited

**Reproduction in whole or in part is permitted
for any purpose of the United States Government**

AD A 006403

UNCLASSIFIED

SECURITY CLASSIFICATION OF THIS PAGE (When Data Entered)

REPORT DOCUMENTATION PAGE		READ INSTRUCTIONS BEFORE COMPLETING FORM
1. REPORT NUMBER	2. GOVT ACCESSION NO.	3. RECIPIENT'S CATALOG NUMBER <i>AD/A-006403</i>
4. TITLE (and Subtitle) SYNERGISTIC AND NOVEL EFFECTS IN COMPOSITE SOLID PROPELLANT COMBUSTION		5. TYPE OF REPORT & PERIOD COVERED Annual Summary Report Sept. 1, 1973-August 31, 1974
7. AUTHOR(s) Warren C. Strahle John C. Handley		6. PERFORMING ORG. REPORT NUMBER
9. PERFORMING ORGANIZATION NAME AND ADDRESS Georgia Institute of Technology Atlanta, Georgia 30332		8. CONTRACT OR GRANT NUMBER(s) N0014-67-A-0159-0016
11. CONTROLLING OFFICE NAME AND ADDRESS Office of Naval Research Power Branch Arlington, Virginia		10. PROGRAM ELEMENT, PROJECT, TASK AREA & WORK UNIT NUMBERS
14. MONITORING AGENCY NAME & ADDRESS (if different from Controlling Office)		12. REPORT DATE October, 1974
		13. NUMBER OF PAGES 68
		17. SECURITY CLASS. (of this report) UNCLASSIFIED
		15. DECLASSIFICATION/DOWNGRADING SCHEDULE
16. DISTRIBUTION STATEMENT (of this Report) Approved for public release; distribution unlimited		
17. DISTRIBUTION STATEMENT (of the abstract entered in Block 20, if different from Report)		
18. SUPPLEMENTARY NOTES		
19. KEY WORDS (Continue on reverse side if necessary and identify by block number) Combustion Hydroxyl terminated Polybutadiene Solid Propellants Catalysts Ammonium Perchlorate		
20. ABSTRACT (Continue on reverse side if necessary and identify by block number) This report summarizes experiments and analysis concerned with sandwich and cast composite solid propellant combustion. The ingredients used in the experiments are ammonium perchlorate as the oxidizer, hydroxyl terminated polybutadiene as the binder and four catalysts: Harshaw catalyst Cu-0202, Fe ₂ O ₃ , ferrocene and iron blue. Cinephotomacrography and the fuze wire technique are used for combustion visualization and burn rate determination. Scanning electron microscopy is used for quenched sample visualization.		

DD FORM 1 JAN 73 1473

ED

Reproduced by
NATIONAL TECHNICAL
INFORMATION SERVICE
US Department of Commerce
Springfield, VA. 22151

UNCLASSIFIED PRICES SUBJECT TO CHANGE
SECURITY CLASSIFICATION OF THIS PAGE (When Data Entered)

UNCLASSIFIED

SECURITY CLASSIFICATION OF THIS PAGE(When Data Entered)

20. (continue abstract)

Areas investigated are a) analytical and experimental determination of synergistic catalytic effects in sandwich and propellant combustion, b) the loading of ferrocene into the binder at the molecular level and its effect on sandwich combustion, c) differential scanning calorimetry of catalyst laden binder and d) analysis of sandwich deflagration.

1a

SECURITY CLASSIFICATION OF THIS PAGE(When Data Entered)

Synergistic and Novel Effects
in Composite Solid Propellant Combustion

W. C. Strahle
J. C. Handley

October 1, 1974

Second Annual Summary Report - Research Sponsored
by
The Office of Naval Research

ONR Contract No. N0014-67-A-0159-0016
Requisition Purchase Request NR 092-543

Approved for Public Release; Distribution Unlimited

Reproduction in whole or in part is permitted
for any purpose of the United States Government

Abstract

This report summarizes experiments and analysis concerned with sandwich and cast composite solid propellant combustion. The ingredients used in the experiments are ammonium perchlorate as the oxidizer, hydroxyl terminated polybutadiene as the binder and four catalysts: Harshaw catalyst CU-0202, Fe_2O_3 , ferrocene and iron blue. Cinephotomacrography and the fuze wire technique are used for combustion visualization and burn rate determination. Scanning electron microscopy is used for quenched sample visualization. Areas investigated are a) analytical and experimental determination of synergistic catalytic effects in sandwich and propellant combustion, b) the loading of ferrocene into the binder at the molecular level and its effect on sandwich combustion, c) differential scanning calorimetry of catalyst laden binder and d) analysis of sandwich deflagration.

ic/

Table of Contents

	Page
Abstract	i
Chapters	
I. Introduction	1
II. Determination of Possible Synergistic Effects	2
a. Two-dimensional Sandwiches	2
b. Cast Composite Propellant	9
III. Indian Head Ferrocent	14
IV. Differential Scanning Calorimetry	18
V. Analytical Efforts	21
VI. Conclusions	27
References	29
Appendix	30
Solid Propellant Sandwich Deflagration Analysis	31
Distribution List	64

I. Introduction

This report summarizes efforts of the second year on contract ONR No. N0014-67-0159-0016. Prior results were concerned with the sandwich configuration and the individual effects of the catalysts Harshaw catalyst CUO202, Fe_2O_3 , ferrocene and iron blue. This year's effort consisted of both sandwich and cast propellant investigations to determine a) possible synergistic catalytic effects whereby for the same total loading of catalyst the effect of two catalysts would be greater than either one alone and b) the behavior of a unique type of ferrocene loading at the molecular level into R-45 prepolymer. Differential scanning calorimeter studies were also performed on catalyst laden hydroxyl terminated polybutadiene (HTPB) binder. Analysis was conducted to explain synergistic catalytic effects and to improve on a previous model of sandwich deflagration.

The reason for investigating synergistic effects is that they were accidentally discovered on the prior year's program. Incorporation of this effect would allow the propellant chemist more flexibility in propellant formulation. The investigation of loading of ferrocene at the molecular level was motivated by prior conclusions that physical loading of catalyst into the binder is a poor way to obtain catalysis. The differential scanning calorimeter work was motivated by prior results that catalysts did not appear to change the pyrolysis mechanism of the binder; a confirmation was desired in other than a deflagration situation. The analysis was required as an aid in reasoning the significance of the experimental results and to see to what degree a sandwich analysis may be used for a cast composite propellant deflagration analysis.

II. Determination of Possible Synergistic Effects

a. Two-Dimensional Composite Solid Propellants

Two-dimensional composite solid propellant sandwiches were used to investigate the optimum location and the extent of the catalytic action of four possible burn rate modifiers.⁽¹⁾ Both the location and the compounds were varied independently. During that investigation it was determined that if one catalyst was added to the oxidizer prior to compaction of the disk and another effective catalyst was added to the binder, there was a net increase of the burn rate over that of the sum of the independent actions of the catalysts. This combined effect is denoted as a synergistic effect on the burn rate. The current study has systematically investigated this positive synergism for all combinations of the same four compounds.

The two-dimensional composite solid propellant sandwiches were prepared by the method outlined in Reference 2 from disks of polycrystalline oxidizer and layers of binder. The disks were pressed from crystalline ammonium perchlorate (AP) in a mold at 30,000 psi. The disks were assembled into multi-layered sandwiches by binding them together with layers of hydroxyl terminated polybutadiene (HTPB). The thickness of the binder layer was maintained at 150 μm during the curing process by using Teflon spacers and spring loaded sample clamps.

The four compounds investigated were Harshaw catalyst CuO2O2, (CC), ferric oxide, (IO), iron blue, (IB), and ferrocene, (F). Harshaw catalyst CuO2O2 is a commercially available catalyst. It is a mixture of approximately 82% cupric oxide, CuO , and 17% chromic oxide, Cr_2O_3 . It is used in accelerating both oxidation and reduction processes. It is commonly referred to as copper chromite. Ferric oxide, Fe_2O_3 , exhibits, as do most

transition element compounds, a high degree of catalytic activity. It is used primarily for oxidation processes. Iron blue is commercially used as a pigment. It is a complex ammonium iron hexacyanoferrate with the chemical formula, $\text{Fe}(\text{NH}_4)\text{Fe}(\text{CN})_6$. It has a cubic crystalline structure. The iron is present as both ferric and ferrous ions in the lattice. Ferrocene is an organometallic compound with the chemical name, bis(cyclopentadienyl) iron, $(\text{C}_5\text{H}_5)_2\text{Fe}$. It is a yellow crystalline solid with relatively high thermal stability for an organometallic compound.

The samples were prepared with constant volumetric loading of the compounds based on an addition of 2w% to the oxidizer. This amount of catalyst was added to the AP prior to grinding and pressing and 4.37w% of catalyst was added to the HTPB.

The cured oxidizer-fuel sandwiches were cut into 8 mm by 4 mm samples. These prepared samples were mounted in the pressurized combustion apparatus of Jones.⁽³⁾ Motion pictures of the burning sample were obtained at a rate of 1600 frames per second at a latent image magnification of 1:1 and 2:1. These motion pictures were used to obtain an accurate value of the sample burning rate. The sandwich vertical burn rate and the burn rate normal to the oxidizer surface, as defined in Reference (1), were obtained for all combinations of the four catalysts along with suitable base line cases at the same volumetric loading in the binder and oxidizer at a combustion pressure of 600 psia.

The tabulated results for the determination of possible synergistic effects are shown in Table 1. The base line comparison cases for a single catalyst present were for 2w% of catalyst added to the AP and 4.37w% of catalyst added to the HTPB. This gave a uniform volumetric loading of

TABLE I. BURN RATES FOR DETERMINATION OF SYNERGISTIC
EFFECTS FOR SANDWICHES AT 600 PSIA.

CATALYST	r	r Cos θ
NONE	.22 in/sec	.21 in/sec
HARSHAW CATALYST CuO2O2 (CC)	.51	.33
FERRIC OXIDE (IO)	.33	.23
IRON BLUE (IB)	.37	.20
FERROCENE (F)	.30	.15
CC & IO	.54	.36
CC & IB	.50	.47
CC & F	.43	.29
IO & IB	.51	.25
IO & F	.44	.36
IB & F	.40	.31

catalyst across the binder-oxidizer interface of the two-dimensional sandwiches. The total weight of the catalyst was maintained constant for the combinations of catalysts. One weight percent of one catalyst along with 1w% of another catalyst was added to the AP and 2.2w% of each catalyst was added to the HTPB. The results obtained for the base line cases of single catalysts added to the sandwiches are in agreement with previous data.⁽¹⁾ It must be noted that the comparison cannot be exact since in the previous investigation⁽¹⁾ the catalyst loading was discontinuous across the binder-oxidizer interface, but in previous experiments catalyst in the binder was shown to be ineffective.

Ferric oxide, iron blue and ferrocene, when used alone, were burn rate inhibitors for AP at 600 psia.⁽¹⁾ The burn rate normal to the oxidizer surface was less than that of the uncatalyzed AP. This is also true in Table 1. When these proven inhibitors of the AP deflagration process were used in combinations with the same total mass of catalyst present, the burn rate normal to the oxidizer surface was increased over that of the uncatalyzed AP. This was noted for the IO-IB, IO-F and IB-F systems. Harshaw catalyst CuO202 increased the AP deflagration rate when used alone at 600 psia. All combinations of Harshaw catalyst CuO202 with the other three compounds exhibited a synergistic effect on the AP deflagration rate even though three of them acted as inhibitors when used alone.

The maximum sandwich burn rate (.54 inches/sec) has been obtained with the combination of Harshaw catalyst CuO202 and ferric oxide. The largest synergistic effect (burn rate change as compared with either single catalyst alone) has been seen for a ferric oxide and iron blue mixture with a burn rate of .51 inches/sec. All combinations of catalysts did give some

degree of positive synergism of the sandwich vertical burn rate. For the combinations with Harshaw catalyst CuO2O2 only ferric oxide was able to clearly increase the burn rate above that of Harshaw catalyst CuO2O2 alone. All combinations of ferrocene in this configuration yielded relatively lower sandwich vertical burn rates.

Considering these results, the most promising two combinations of catalysts, Harshaw catalyst CuO2O2 - ferric oxide and iron blue - ferric oxide were chosen for testing over the pressure range of 300 to 2000 psia.

The results for the Harshaw catalyst CuO2O2-ferric oxide system tests are shown in Figure 1. The maximum effect is at 1500 psia. Both catalysts were equally effective in catalyzing the burn rate when used alone. When half of one catalyst was replaced by the same amount of the second catalyst the burn rate doubled. The sandwich vertical burn rate and the burn rate normal to the oxidizer surface both exhibited positive synergism over the entire pressure range.

For the iron blue - ferric oxide samples the results were not as clear. They are shown in Figure 2. The maximum positive effect occurs at 600 psia. It is not conclusive at 1000 and 1500 psia that a positive synergistic effect has been obtained, since the combined catalysts produce a burn rate that lies between the burn rates obtained for a single catalyst present. A negative effect has not been produced, i.e. the burn rates have not been inhibited. Within the experimental accuracy of the test the burn rate normal to the oxidizer surface for the combined catalysts loading has followed the burn rate for ferric oxide.

As in previous tests the separation between the dashed and solid curves is representative of the amount of catalytic activity taking place in the

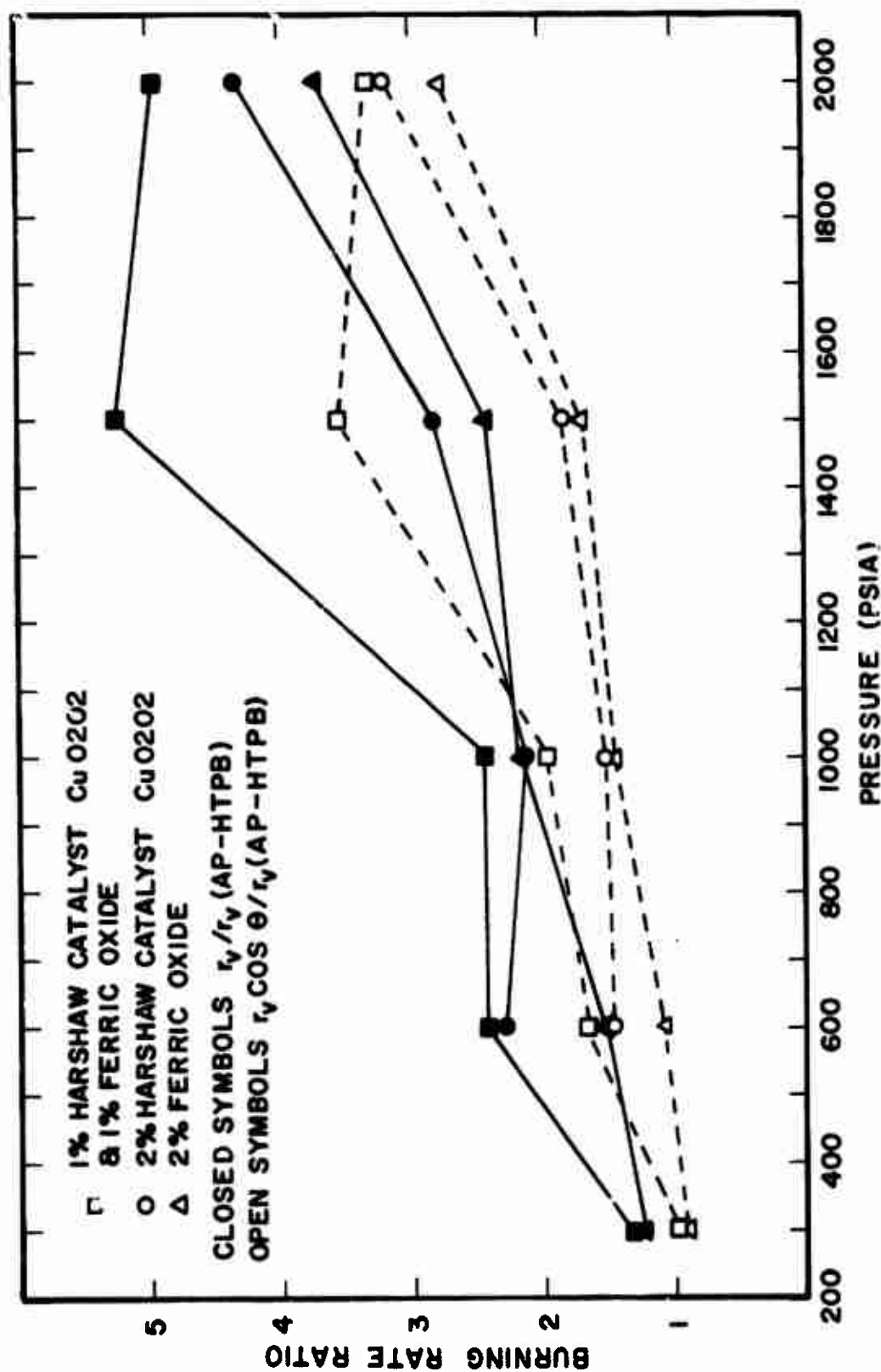


FIGURE 1. BURN RATE RATIO FOR HARSHAW CATALYST CuO₂O₂ AND FERRIC OXIDE.

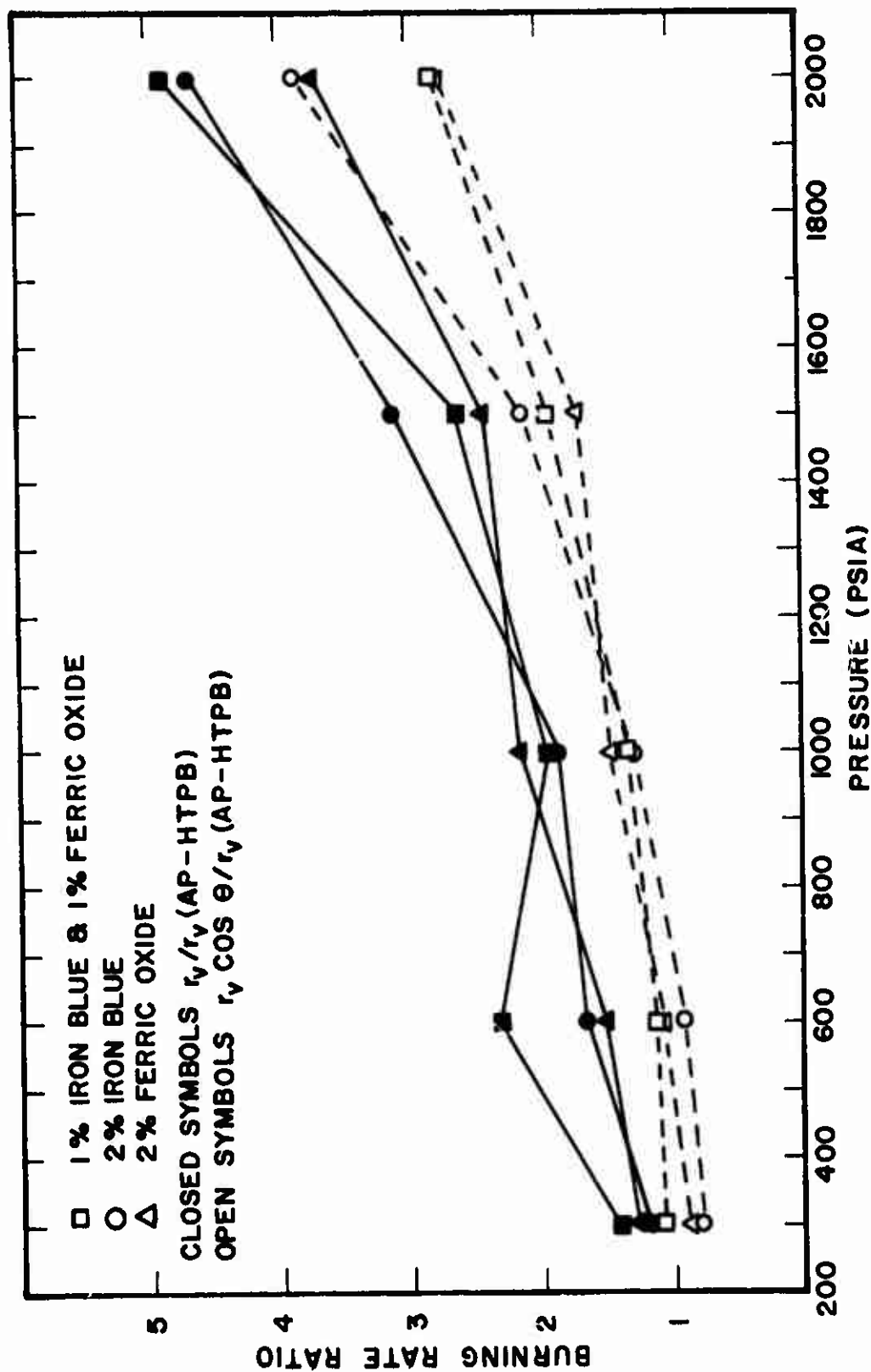


FIGURE 2. BURN RATE RATIO FOR IRON BLUE AND FERRIC OXIDE.

binder-oxidizer reactions. The tests that showed large positive synergistic effects, Harshaw catalyst CuO 202 and ferric oxide at 1500 and 2000 psia, and iron blue and ferric oxide at 600 and 2000 psia, also showed substantial increases in this separation of the two burn rates.

b. Cast Composite Propellants

Maintaining the same volumetric loading of catalysts as for the two-dimensional sandwiches, three-dimensional cast composite solid propellant strands were prepared to see if this synergistic effect would be carried over to the real cast propellant. These strands were prepared from a common lot of uncured composite propellant with an 83%/17% solids to binder loading. The oxidizer was chosen to have a bimodal ammonium perchlorate particle distribution of 30% 40 μm and 70%, 180 μm . The binder was hydroxyl terminated polybutadiene. Burning rate data are available for this uncatalyzed propellant.⁽⁴⁾ It was similar to propellant #78 in the Princeton University test series. The catalyst was added to the uncured propellant at a weight percent of 2.41. This would give the same equivalent volumetric loading as in the sandwiches.

The strands were cast in teflon molds and all samples were cured for the same length of time. The strand size was .25 inch by .25 inch by 1.7 inches long. The burn rates were obtained by a fuse wire technique⁽⁴⁾ using seven, $\frac{1}{2}$ ampere ($\sim .010$ inch diameter), wires inserted in predrilled holes which were spaced .2 inches apart. Each fuse wire was connected in series to a 10 K Ω resistor. These seven resistors were connected in parallel with a 57 K Ω resistor across an 18 volt battery power supply. As each fuse wire burns through the equivalent resistance increases and the

voltage is recorded on an oscillograph.

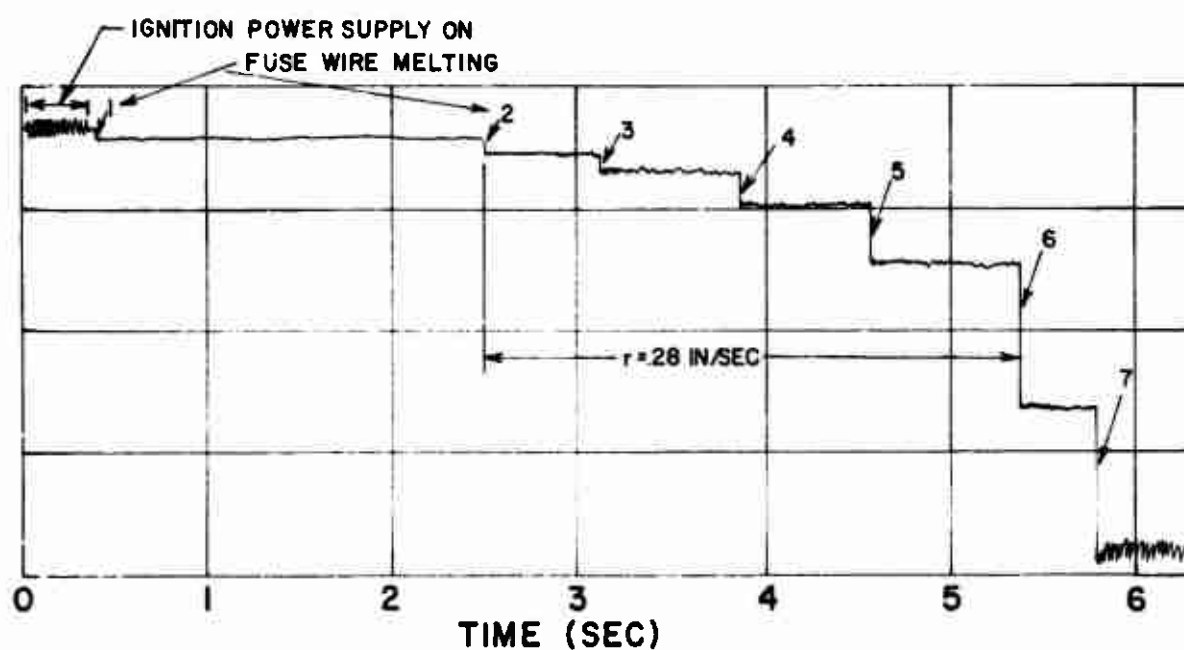
The strand with fuse wires is shown in Figure 3. It is mounted on the base of the combustion bomb. A sufficient nitrogen flow is passed over the sample to prevent recirculation of the hot gases that can cause premature melting of the fuse wires. This nitrogen flow has varied from .7 to 1.4 ft/sec. The most stable results were obtained at the higher flow rates. Sample oscillograph traces are shown in Figure 4 for an uncatalyzed strand and one with ferric oxide added to the strand.

The burn rates for the addition of the two most promising combinations of catalysts as determined from the two-dimensional composite solid propellant test are tabulated in Table 2. These strands of propellant were burned at 600 psia. For the combination of ferric oxide and iron blue, the burn rate is between the burn rates of the samples with only one catalyst present. The ferric oxide - Harshaw catalyst CuO2O2 system showed a reduction of burn rate below that of either of the two catalysts used alone.

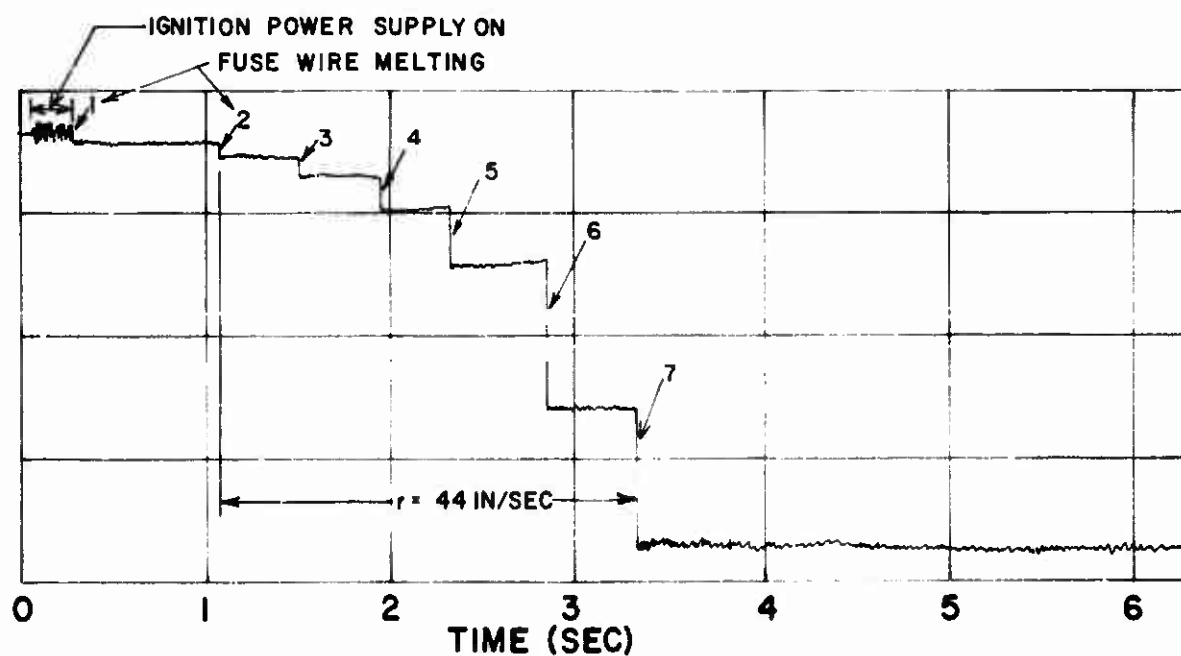
The burn rates do not compare favorably with the results obtained in Table 1 for the two-dimensional sandwiches. The burn rate for the uncatalyzed strands agree with the Princeton data. The structural strength and elasticity of the samples containing both Harshaw catalyst CuO2O2 and iron blue were considerably different from the ferric oxide and pure samples. The ferric oxide and pure samples were softer and more easily removed from the mold while the samples containing iron blue and Harshaw-catalyst CuO2O2 were brittle and exhibited several tests with very rapid burning. These tests were not considered in the preparation of Table 2.



FIGURE 3. A STRAND WITH SEVEN FUSE WIRES MOUNTED ON THE COMBUSTION BOMB BASE.



a) AP - HTPB NO CATALYST.



b) AP - HTPB 2.41 w% FERRIC OXIDE.

FIGURE 4. OSCILLOGRAPH RECORDS FOR TWO STRANDS.

TABLE II. BURN RATES FOR CAST COMPOSITE PROPELLANT STRANDS.

CATALYST	r
<p>NONE</p> <p>HARSHAW CATALYST CuO2O2 (CC)</p> <p>FERRIC OXIDE (IO)</p> <p>IRON BLUE (IB)</p>	<p>.28 in./sec</p> <p>.50</p> <p>.44</p> <p>.36</p>
<p>CC & IO</p> <p>IO & IB</p>	<p>.41</p> <p>.43</p>

These cast propellant samples were initially prepared to contain on average the same volumetric loading of catalyst as the sandwiches. But for the cast propellants all of the catalyst is suspended in the binder matrix, which constitutes 17w% of the sample. Since 2.41w% of catalyst was added to the cast propellant samples, the binder matrix contains 14.2w% of the catalyst. The binder matrix for the sandwiches contained 4.4% of catalyst. This increase of catalyst in the binder effected the cure and the strength of the binder. This high catalyst loading in the binder may be above the amount required for maximum burn rate augmentation. It was determined earlier⁽¹⁾ that the addition of the catalyst directly into the polycrystalline structure was more effective than addition to the binder. If the catalyst could be distributed in the oxidizer crystalline structure to give the same volumetric loading as in the sandwiches a more realistic comparison could be made. This would require a development of a new ammonium perchlorate production technique. It may be possible to establish the existence of a synergistic effect in cast propellants if the total catalytic loading in the binder is reduced to a more comparable level with the two-dimensional sandwiches. This approach will be followed in future efforts.

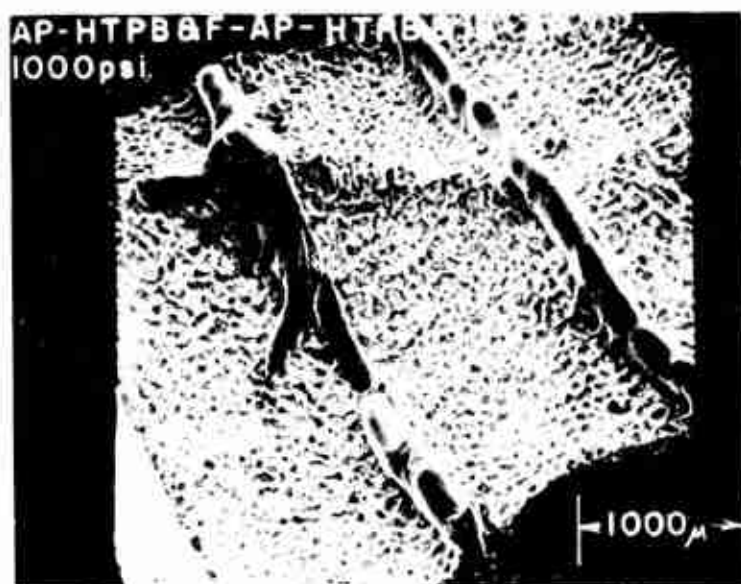
III. Indian Head Ferrocene

It had been a prior conclusion^{(1), (2)} that crystalline catalysts physically loaded into the binder were ineffective in augmenting sandwich deflagration rates. The apparent reason is that with the catalyst in the binder the diffusion of crystalline matter, once it is released into the gas phase, toward the hot AP is too slow to augment the binder-oxidizer

reactions fast enough to increase heat feedback to the sandwich surface. Furthermore, the dispersion of catalytic material must be greater for a substance dispersed at the molecular level rather than at a macroscopic crystalline level. Following this hypothesis, it would be desirable to introduce the catalyst in molecular rather than crystalline form, once the binder had pyrolysed to the gas phase. The diffusion of gas phase molecules should be faster than crystalline particles.

It was learned that the Naval Ordnance Station at Indian Head, Maryland was working in the area of chemically loading ferrocene into R-45 polymer.⁽⁵⁾ Indian Head supplied some of the polymer with 5% Fe by weight in the polymer. Due to an advanced state of cure of the received material work with this substance was limited, but one sandwich was prepared with this material.

Figure 5 shows scanning electron microscope pictures of quenched samples burned at 1000 psia. One sample shown is from prior work with the crystalline ferrocene in the binder alone and the other sample is with the Indian Head ferrocene. The striking effect of the chemically loaded ferrocene is the depression of the AP in the vicinity of the oxidizer-binder interface. This is interpreted, as shown by many past results, as increased chemical rates between the binder and oxidizer for the Indian Head binder as compared with the binder with crystalline catalyst. Because the AP is not flat (horizontal) the vertical burn rate of the sandwich had to be greater with the Indian Head binder. This result is considered to confirm the hypothesis of molecular diffusion and greater dispersion as explained above.

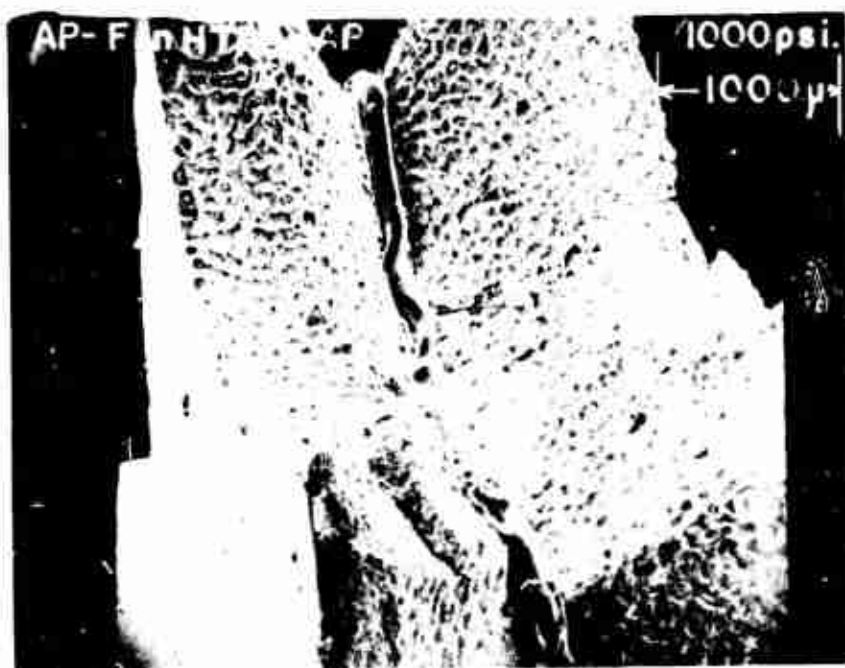


a) Ferrocene Mixed in HTPB x 27

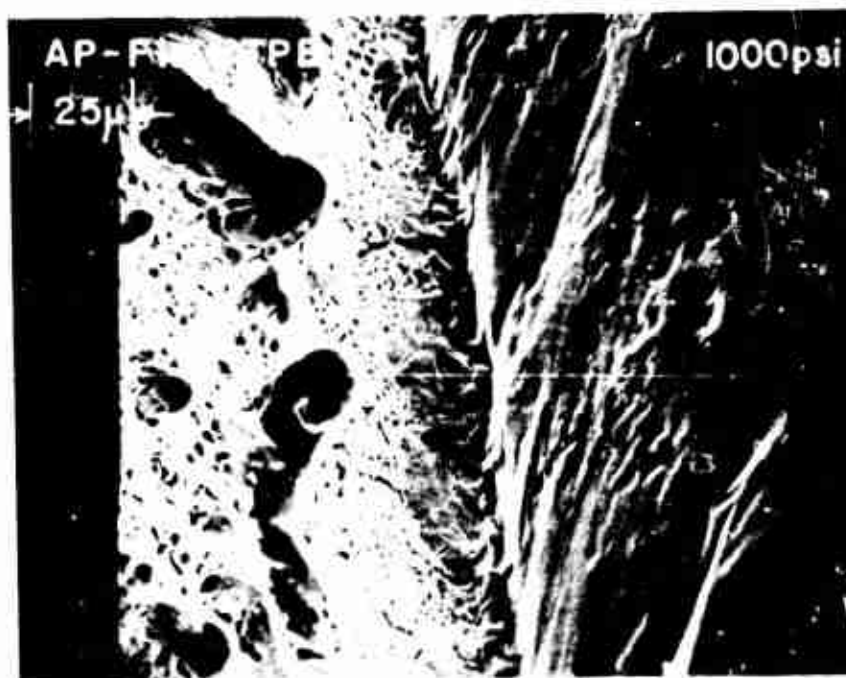


b) Ferrocene Mixed in HTPB x 126

FIGURE 5. (a) AP-HTPB&F 1000psi (b) AP-HTPB&F 1000psi FERROCENE IN THE BINDER.



c) Ferrocene in R45 M Component of HTPB x 25



d) Ferrocene in R45 M Component of HTPB x 56

FIGURE 5. VIBRATION MICROGRAPHS OF CASTING WITH FERROCENE IN THE BINDER.

IV. Differential Scanning Calorimetry

Since prior sandwich results led to the conclusion that catalytic effectiveness is poor when the catalyst is loaded into the binder, and there has been no evidence that catalysts increase the binder pyrolysis rate, it was desired to check these conclusions by differential scanning calorimetry applied to catalyst-laden binder. The apparatus used was a Perkin-Elmer Differential Scanning Calorimeter, Model DSB-1B, and the procedures used were identical to those of Ref. 6. The binder used was HTPB and two catalysts, iron blue and ferrocene, were investigated. The nominal weight of each sample was 5 mg. and the amount of catalyst loading was consistent with that used in the sandwich deflagration tests, 4.4w%

The DSC unit measures the difference in power required to heat two samples, one inert and one containing the decomposing sample, through a programmed temperature rise. Sample graphs, shown on Figure 6 are two HTPB runs at a scan rate of 5 K/min. This figure shows the reproducibility attainable between runs. The heat of gasification is $q = \int_0^{\infty} \dot{Q} dt = \int_{T_0}^{T_f} \dot{Q} (1/dT/dt) dt$ where T_f is the temperature at which gasification for pure HTPB are shown in Table 3. In Table 3 there is a high degree of data scatter but an unmistakable trend of heat of gasification with scan rate dependent. A plot of q v.s. $1/\text{scan rate}$ is given in Figure 7. A line through the most consistent set of data (HTPB-IB) shows an extrapolation to infinite scan rate of $q = 265 \text{ cal/g}$. This should be compared with 433 cal/g obtained in Ref. 7, which was obtained at heating rates comparable to those found during propellant deflagration,

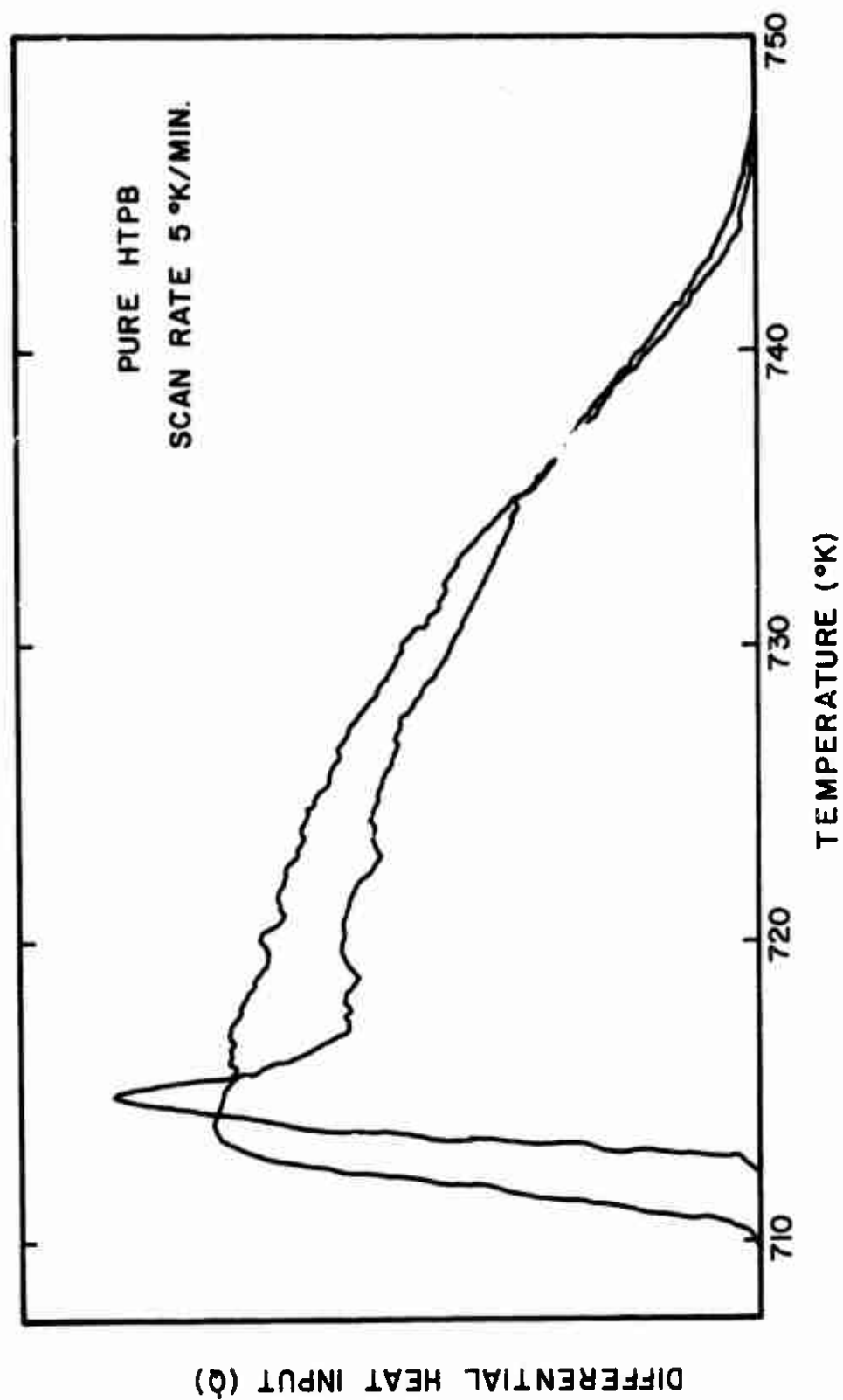


FIGURE 6. DIFFERENTIAL HEAT INPUT AS A FUNCTION OF TEMPERATURE .

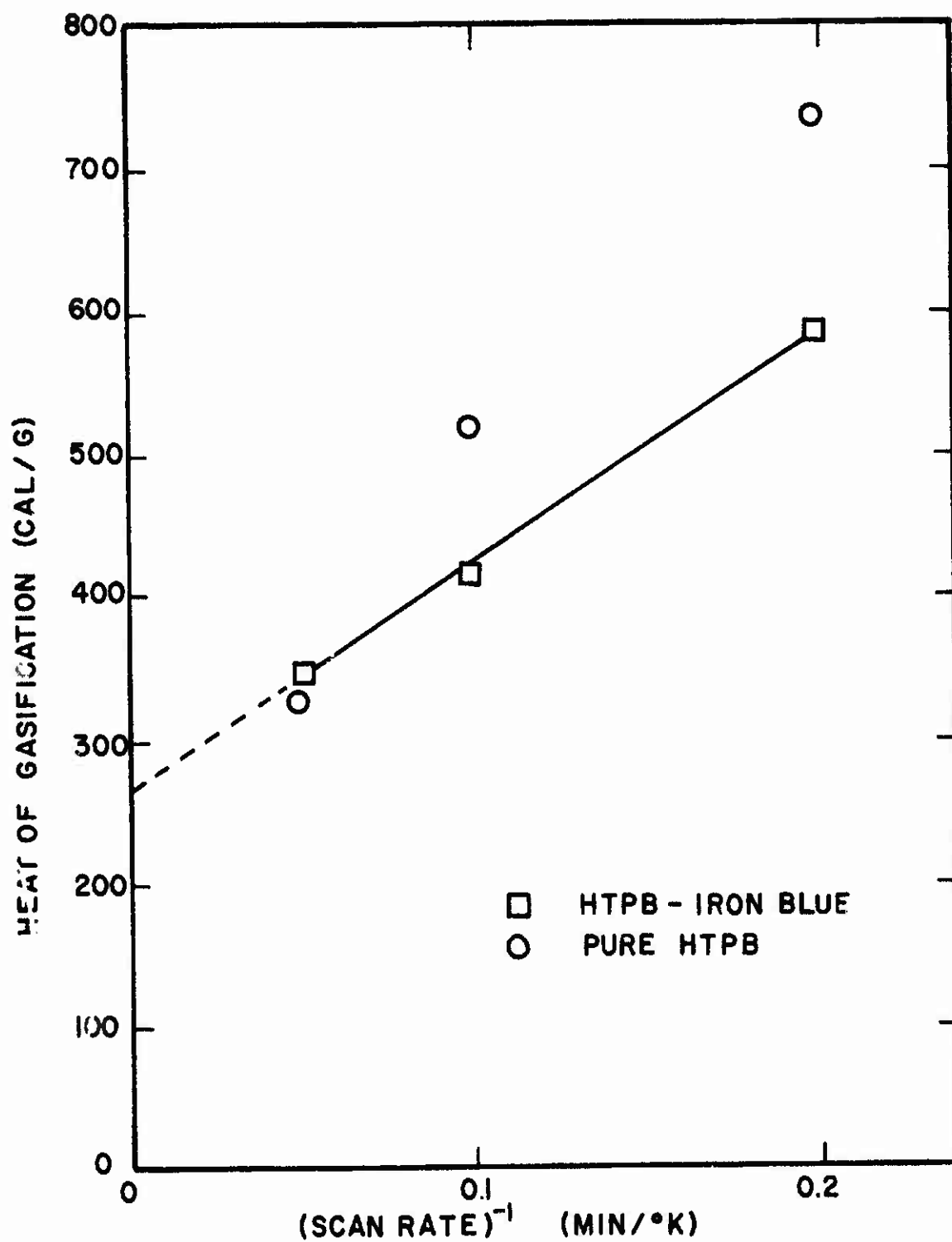


FIGURE 7. HEAT OF GASIFICATION AS A FUNCTION OF THE RECIPROCAL SCAN RATE.

Table 3

Heat of Gasification for HTPB and HTPB - catalyst

Scan Rate (K/min)	Binder	No. of Tests	q (cal/g)
20	HTPB	1	328
10	HTPB	3	518 \pm 75
5	HTPB	2	735 \pm 129
20	HTPB-IB	1	345
10	HTPB-IB	5	415 \pm 94
5	HTPB-IB	1	584
20	HTPB-F	1	285

which are orders of magnitude higher than may be found with the DSC unit. The primary conclusion, however, is that within the data scatter there appears no definite effect of IB or F on the heat of decomposition of HTPB.

Figures 8 and 9 show the actual traces for pure HTPB and HTPB-IB at scan rates of 10 K/min. The catalyst has very little effect upon the temperature at the onset of decomposition activity. There does appear, however, to be a minor effect of IB in smoothing out the roughness near the peak of the decomposition activity. Nevertheless, the overall temperature width of activity and the heat of gasification is affected in only a minor way. The same conclusion may be derived from the HTPB-F run.

V. Analytical Efforts

Two major analytical efforts have been conducted during the current year. One task concerned an explanation of synergistic effects and the other concerned an extension of a previous sandwich deflagration analysis.⁽⁸⁾ During the course of extension of the sandwich analysis, two major items were discovered: a) the solution procedure used in the previous effort was

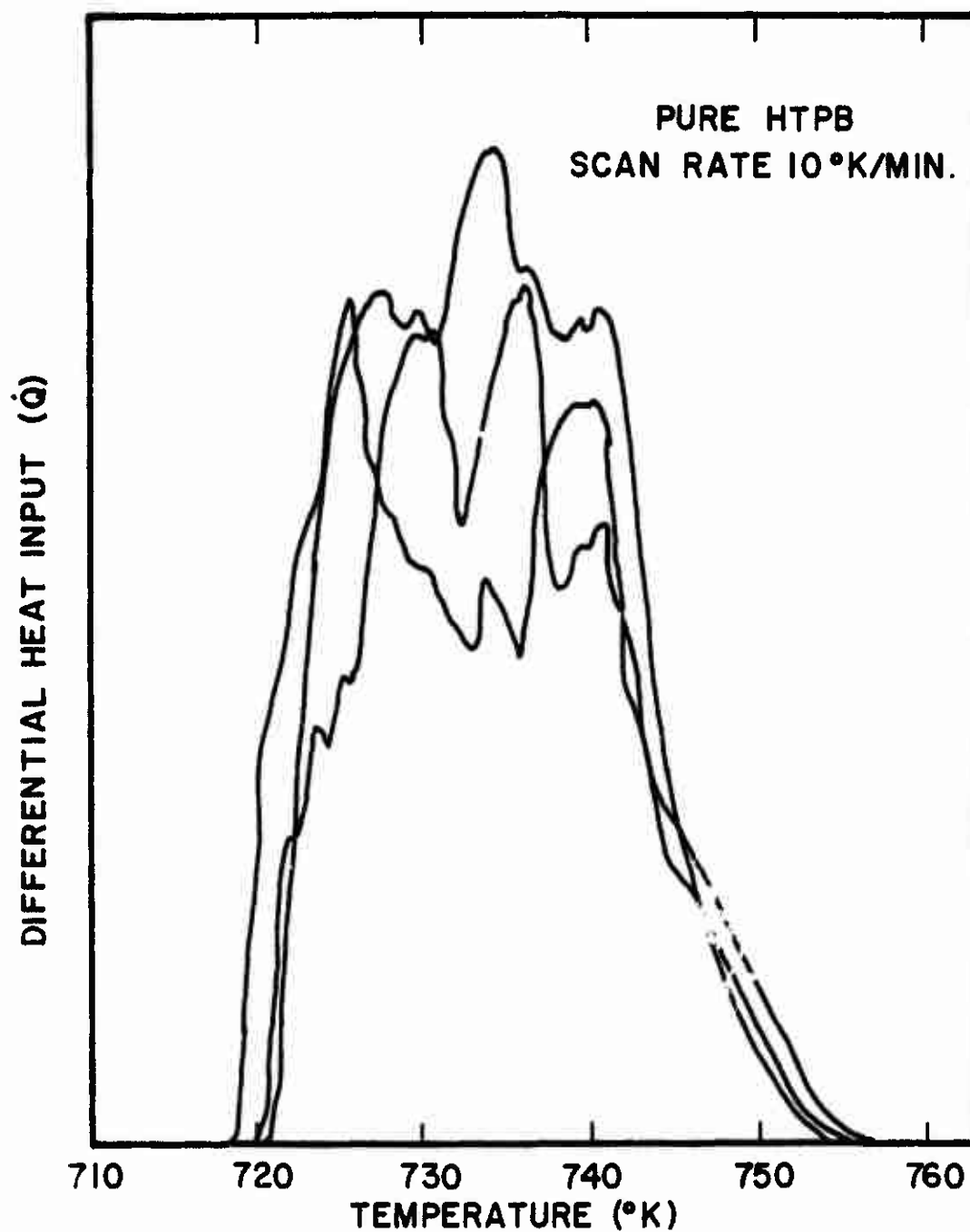


FIGURE 8. DIFFERENTIAL HEAT INPUT AS A FUNCTION OF TEMPERATURE.

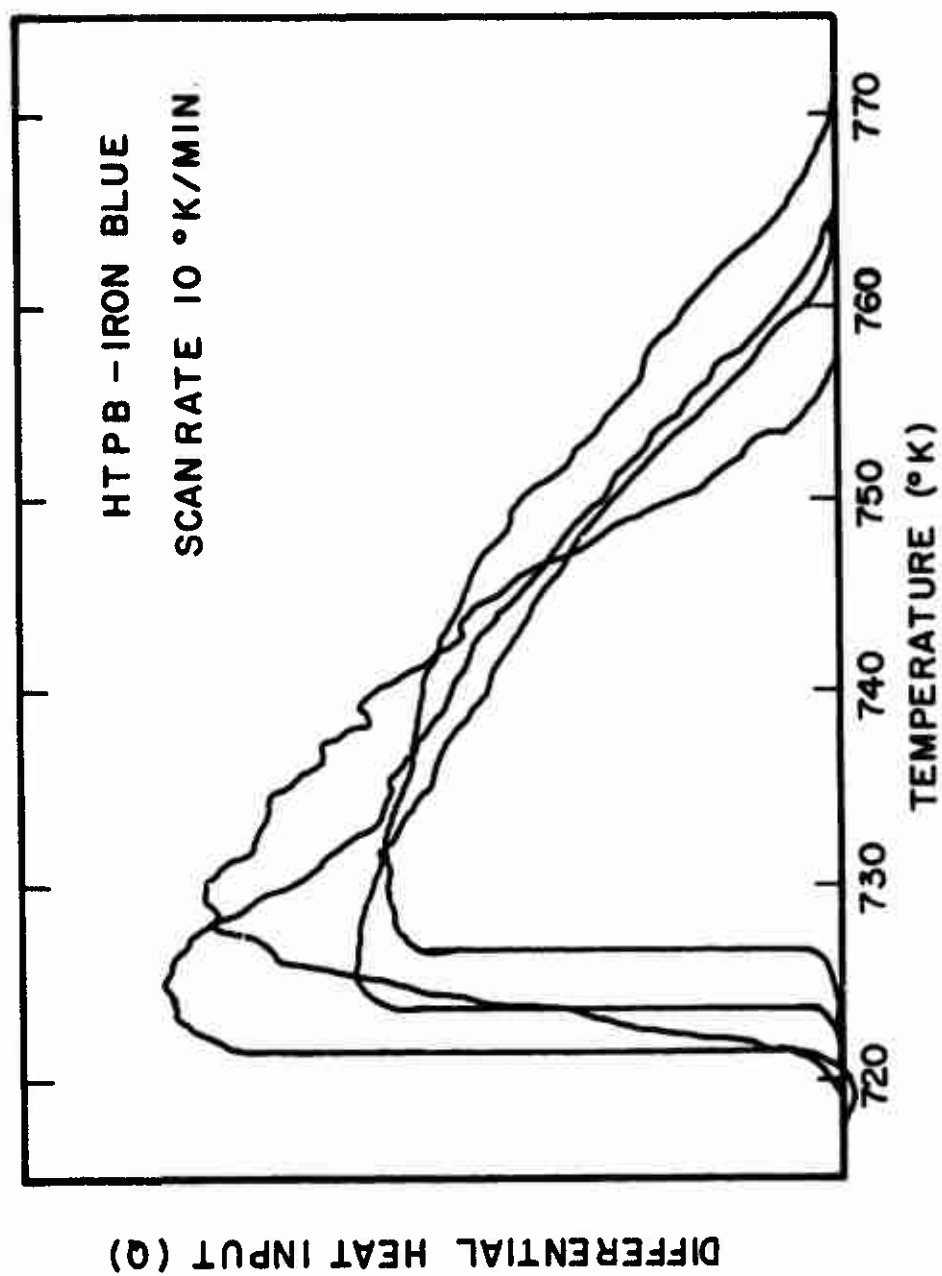


FIGURE 9. DIFFERENTIAL HEAT INPUT AS A FUNCTION OF TEMPERATURE.

in error and b) an improved solution could be found for the solid phase heat transfer problem. As a consequence it was found that the sandwich burn rate, which could not be found with the old procedure, appears as an eigenvalue to the problem. The restricted problem of an inert, dry binder adjacent to deflagration AP was therefore solved by the new procedure. The details are located in the Appendix.

Synergistic effects were first treated by insertion of two catalytic reactions in the chemical kinetics scheme of Ref. 9 for deflagrating AP. It is believed that the details should not be presented here because it may be construed that these catalytic reactions are being proposed as actual catalytic mechanisms; whereas, they were only introduced as a plausibility argument for synergistic effect. The plausibility argument which is presented here encompasses all of the results that were obtained from the AP deflagration model without confusing the issue with AP details.

To explain the results of the AP catalysis model on a simple basis the effect of two catalysts on the reaction rate, R , may be modeled as follows:

$$R_a = R_o f_1(Y_{c_1}) f_2(Y_{c_2}) \quad (1)$$

or

$$R_b = R_o + g_1(Y_{c_1}) + g_2(Y_{c_2}) \quad (2)$$

where the f 's and g 's as functions of the catalyst mass fraction, Y_c , are shown in Figure 10. Equations (1) and (2) merely represent two functional assumptions which yield expected behavior with respect to each catalyst. There is a general rise in rate with catalyst loading to a maximum, and a fall off in rate to zero must occur as the catalyst, which is inert, saturates the propellant. Since the burn rate is roughly proportional to

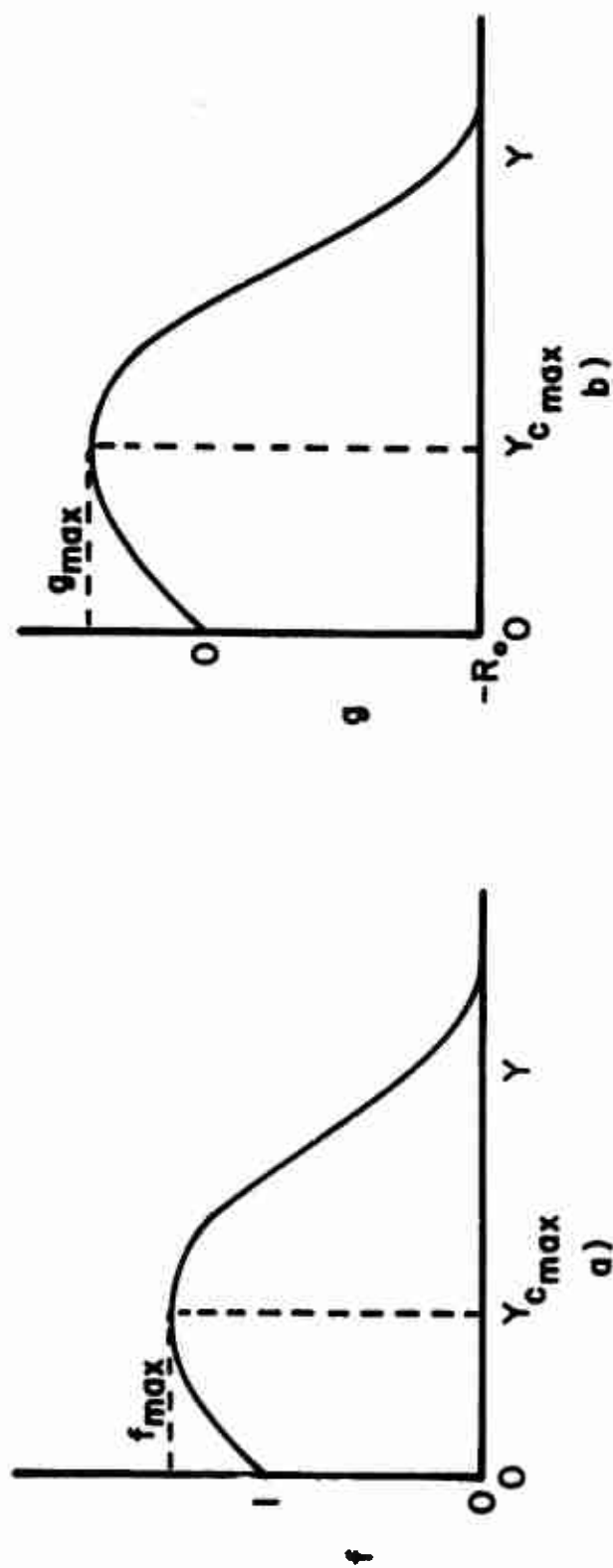


FIGURE 10. SAMPLE CATALYTIC RATE FUNCTIONS.

the square root of the reaction rate,⁽¹⁰⁾ Eqs. (1) and (2) yield the two options for the burn rate:

$$r_a = KR_a^{\frac{1}{2}} \quad r_b = KR_b^{\frac{1}{2}} \quad (3)$$

where K is some constant. As long as the shape of the rate curves in Figures 10a and 10b is as shown, the following conclusions are valid:

$$a) \quad r(Y_{c_1}, Y_{c_2}) > r(Y_{c_1}, 0) \text{ or } r(0, Y_{c_2}) \text{ for } Y_c \leq Y_{c_{\max}}$$

$$\text{and } b) \quad r_{\max} = r(Y_{c_1_{\max}}, Y_{c_2_{\max}}).$$

In this case the addition of a second catalyst will always augment the rate above what may be accomplished with a single catalyst. Moreover, for a fixed total mass of catalyst,

$$Y_{c_1} + Y_{c_2} = c,$$

and for equally effective catalysts so that

$$f_1 = f_2 \text{ or } g_1 = g_2$$

$$r(Y_{c_1}, c - Y_{c_1}) > r(c, 0) \text{ or } r(0, c),$$

as long as

$$c < Y_{c_1_{\max}} = Y_{c_2_{\max}}.$$

Therefore, with the appropriate restrictions, this simple demonstration shows that the presence of one catalyst augments the effect of the presence of another catalyst. This is a synergistic effect upon rate. Of course,

this is only a plausibility argument and no claim is being made that this is the actual mechanism or that Eqs. (1) and (2) are generally valid.

VI. Conclusions

1. All possible combinations of the four catalysts investigated exhibited a positive synergistic effect on the sandwich vertical burn rate when tested at 600 psia and a constant volumetric loading based on a total of 2w% addition of catalyst to the oxidizer.

2. The maximum sandwich burn rate at 600 psia was obtained for the combination of Harshaw catalyst $\text{CuO} \cdot 2\text{O}_2$ and ferric oxide. When these samples were investigated over the pressure range of 300 to 2000 psia, the maximum synergistic effect occurs at 1500 psia. There was a positive synergistic effect over the entire pressure range.

3. The maximum synergistic effect with the two-dimensional sandwiches at 600 psia was obtained for the iron blue and ferric oxide combination. This combination was not as effective as the Harshaw catalyst $\text{CuO} \cdot 2\text{O}_2$ and ferric oxide over the entire pressure range.

4. The cast composite propellant strands did not exhibit a positive synergistic effect when tested at 600 psia.

5. It is suspected that the heavy catalyst loading is responsible for the absence of synergistic effects in the cast propellants. A lower overall loading should be investigated.

6. From testing of ferrocene loaded into R-45 polymer at the molecular level it is concluded that molecular loading of a catalyst into a propellant is superior to physical loading of a crystalline material, as suspected from previous sandwich testing.

7. Differential scanning calorimetry of iron blue and ferrocene-loaded HTPB confirms earlier conclusions that these catalysts do not modify the pyrolysis mechanism of the binder to an appreciable extent.

8. For dry inert sandwiches analysis indicates that in the pressure range of 20 to 100 atm the sandwich should burn with a nearly flat surface and very close to the AP deflagration rate, as has always been observed for uncatalysed sandwiches with even wet binders.

9. A sharp slope discontinuity is predicted at the binder-oxidizer interface for dry binders, as has been seen experimentally for catalysed sandwiches.

10. For typical particle sizes of the order of 20 μm and larger the sandwich analysis can form the basis for a composite propellant deflagration theory, if the binder is dry.

References

1. Strahle, W. C., Handley, J. C., and Kumar, N., "Catalytic Behavior in Solid Propellant Combustion," Annual Summary Report for ONR Contract No. N0014-67-0159-0016. Georgia Institute of Technology, Atlanta, Georgia.
2. Strahle, W. C., Handley, J. C., and Milkie, T. T., "Catalytic Effects in the Combustion of AP-HTPB Sandwiches to 3200 psia," Combustion Science and Technology, Vol. 8, p. 297, (1974).
3. Jones, H. E., "An Experimental Investigation Relating to the Combustion Mechanism of Ammonium Perchlorate Composite Propellants," Ph.D. Dissertation, Georgia Institute of Technology, (1971).
4. Steinz, J. A., Stang, P. L., and Summerfield, M., "The Burning Mechanism of Ammonium Perchlorate-Based Composite Solid Propellants," AMS Report No. 830, ONR Contract Nonr 1858(32), February, 1969.
5. Gotzmer, C., Jr., "Modification of Propellant Binders: Quarterly Progress Report for 15 December 1971 through 15 March 1972," Indian Head Memorandum Report, 72-178, 18 March, (1972).
6. Varney, A. M., "An Experimental Investigation of the Burning Mechanisms of Ammonium Perchlorate Composite Solid Propellants," Ph.D. Dissertation, Georgia Institute of Technology, (1970).
7. Cohen, N. S., Fleming, R. W., and Derr, R. K., "Role of Binder in Solid Propellant Combustion," AIAA Paper No. 72-1121, (1972).
8. Strahle, W. C., "Solid Propellant Sandwich Deflagration Analysis," AIAA Paper No. 74-123, (1974).
9. Guirao, C. and Williams, F. A., "A Model for Ammonium Perchlorate Deflagration between 20 and 100 atm," AIAA Journal, 9, (1971), 1345-1356.
10. Culick, F. E. C. and Dehority, G. L., "An Elementary Calculation for the Burning Rate of Composite Solid Propellants," Combustion Science and Technology, 1, (1969), 193-204.

Appendix

Solid Propellant Sandwich Deflagration Analysis

SOLID PROPELLANT SANDWICH DEFLAGRATION
ANALYSIS

Warren C. Strahle*

Georgia Institute of Technology, Atlanta, Ga.

ABSTRACT

A theoretical solution has been obtained for the shape of a deflagrating ammonium perchlorate surface when it is adjacent to an inert, pyrolysing, dry binder. The eigenvalue, the regression rate, is shown to be independent of binder type and very close to the burn rate of pure AP, as has been experimentally observed. A slope discontinuity of the surface should exist at the binder-oxidizer interface and typical binders should incline very near to 90° to the nearly horizontal AP surface, at the junction of the two. The transition from AP to binder should take place on a distance scale of the order of microns and all results are quite insensitive to pressure level.

This work was sponsored by the Office of Naval Research, Power Branch, under Contract No. N00014-67-0159-0016. Substantial aid in the calculations was given by Mr. Narendra Kumar.

Index categories: Combustion in Heterogeneous Media, Solid and Hybrid Rocket Engines.

*Professor, School of Aerospace Engineering, Member AIAA.

NOMENCLATURE

a	$g + 2q_R Y_F$
b	pyrolysis law constant of vapor pressure constant
\tilde{b}	dimensionless pyrolysis law constant or vapor pressure constant
c_s	solid phase specific heat
c_p	specific heat at constant pressure for gas phase
c	flame standoff distance
C	deviation of c from planar AP case
E	activation energy
g	T/T_0
G	deviation of temperature from planar AP case
G_0, G_1	solid phase temperature perturbation constants
k	preexponential factor in reaction rate law
\tilde{k}	dimensionless preexponential factor in reaction rate law
m, m_g	constants in eigensolution
n	coordinate normal to the solid-gas interface directed toward the gas phase
p	pressure
Q	reaction integral defined by Equations (18)
q	exothermic reaction heat in gas phase, endothermic in solid phase
R	universal gas constant
Re	Reynolds number
r, r_n	burn rate and regression rate normal to surface, respectively
T	temperature
v	gas velocity in y direction

w_F	production rate of NH_3
x, y	coordinates
Y	perturbed y position of solid surface
Y_k	mass fraction of species k
y	deviation of mass fraction from planar AP case
z	$1 + (dy_s/dx)^2$
α	thermal diffusivity, $\lambda/\rho c$
δ	inclination angle of binder
e	dimensionless activation energy, E/RT
η	c_s/c_p
λ	thermal conductivity
ξ	$c_p \lambda_s / c_s \lambda_g$
ρ	density
θ	inclination angle of solid AP surface

Subscripts

B	binder
f	flame temperature
F	NH_3
g	gas phase
o	cold solid
s	solid phase or surface
l	quantity evaluated at flame standoff position

Superscripts

$-$	quantity evaluated for the one-dimensional AP deflagration
-----	--

- ' ordinary derivative with respect to x
- * dimensional quantity
- Λ solid phase perturbation function

INTRODUCTION

A substantial number of experimental investigations of composite solid propellant ingredient behavior have dealt with the sandwich configuration (1-8). By a sandwich is meant a slab of oxidizer, usually ammonium perchlorate (AP) in the cited investigations, adjacent to a slab of polymeric fuel. This two-dimensional configuration is an important experimental configuration for the study of phenomena taking place near the binder-oxidizer interface during a deflagration process. By removing the difficulties of viewing the interface details in a real three-dimensional composite solid propellant, much information has been gathered concerning the behavior and existence of binder melts, catalytic additives, the relative importance of AP-binder reactions in driving the deflagration rate, fluid mechanical instabilities during deflagration, and the behavior of aluminum when placed into the sandwich.

In contrast to the many experimental studies there have appeared no analyses of the sandwich deflagration process with AP oxidizer which had as a goal the prediction of the actual shape of the gas-condensed phase interface. Bakhman and Librovich⁽⁹⁾ theoretically investigated a semi-infinite slab of oxidizer adjacent to a semi-infinite slab of fuel, but the oxidizer was not assumed to be capable of self-deflagration. Nachbar⁽¹⁰⁾ investigated a periodic, two-dimensional array of oxidizer and fuel slabs as a model of an actual propellant. The goal was to predict a mean deflagration rate without predicting an actual achieved two-dimensional surface shape. Again, the oxidizer was assumed incapable of self-deflagration.

The need for an analytical model capable of prediction of the surface shape for an AP oxidized sandwich becomes apparent when trying to reason the behavior which is experimentally observed. Even in this two-dimensional configuration the problem is highly complex due to a) the appearance of binder

melts, b) three phase heat transfer and one phase (perhaps two phase) mass transfer, c) two-dimensional heat and mass transfer, d) non-linearities in the governing equations due to at least chemical reaction and an unknown surface shape, e) multiple chemical reactions and condensed phase reactions, f) a mathematically elliptic problem in an infinite region and g) the appearance of an eigenvalue - the deflagration rate. Under these difficulties an attempt to reason on a qualitative basis, given experimental information, is hampered by the lack of some computational framework and predictive capability.

A previous initial step toward providing a theory of the sandwich deflagration process⁽¹³⁾ failed to yield the burn rate as an eigenvalue of the problem. Furthermore, an analytical error has been discovered in that treatment and the results are consequently in error. The current treatment corrects the error and recovers the burn rate as an eigenvalue of the problem by a more complex solution of the problem.

From a practical standpoint there are two major reasons for treating this problem. The first is to obtain an idea of the distance scales involved in the problem. That is, how far do the influence of the binder and oxidizer penetrate into each other? If these distance scales are small enough, this interface theory may be used in theory of an actual propellant. Secondly, the actual burn rate is desired. Is the influence of the binder on the self-deflagrating AP strong or weak? The current analysis addresses these issues.

ANALYSIS

Model Construction and Assumptions

Given the complicated nature of the problem, a model is first sought which uses available experimental information liberally but which still does not overly restrict the model in interpretation of experimental results. Accordingly, the initial model uses the following observations:

a) Far from the binder-oxidizer interface the AP regresses as pure AP. Furthermore, for binder thicknesses of the order used in some of the experimental studies ($\approx 150 \mu\text{m}$) there is little effect of one side of a sandwich upon the other side even when dissimilar materials are used. Therefore, the initial model development is concerned with a semi-infinite slab of AP against a semi-infinite slab of binder.

b) A steady state is achieved experimentally with AP oxidizer. Consequently, time dependence is assumed absent.

c) For uncatalyzed sandwiches the experimental results show very little effect of the binder-oxidizer reactions upon the surface profile. That is, the heat feedback from the binder-oxidizer reactions does not drive the overall deflagration rate; the AP self-deflagration is responsible for the overall deflagration rate at pressures removed from the low pressure deflagration limit and below 2000 psia. The initial model is therefore constructed assuming binder-oxidizer reactions to have negligible rate. This does not mean that a diffusion flame between the binder and oxidizer is absent, but it means this flame is not close enough to the interface to play a role in the deflagration behavior. Furthermore, the effect of catalysis is not treated.

The initial model therefore asks the question of the surface shape

attained by a semi-infinite slab of AP which pyrolyzes a semi-infinite slab of binder. Posed in this manner it is immediately recognized that the problem has neither a unique solution nor a steady solution because a) the final shape would depend upon the geometry of ignition and b) it would take an infinite time to establish a steady profile in a semi-infinite slab of inert binder. The ignition problem is seen by imagining two cases - one in which ignition is achieved by a line heat source (say an ignition wire) and a second in which ignition is achieved uniformly over the entire AP surface. In the first case the AP would take on the shape of ever-increasing circular radii from the ignition point. In the second case the AP would deflagrate in a planar fashion except in the vicinity of the binder. However, these comments neglect the fact that the inert nature of the binder may affect the shape attained by the AP, even far away from the binder. Surely, at long enough time the profile in the interface vicinity will have become shape-invariant, but it is not obvious that the AP will be horizontal (assuming top-to-bottom deflagration). In fact, this is to be determined by the solution. Concerning the binder, it appears clear that after a sufficiently long time the processes in the interface vicinity will not depend upon processes taking place at a large vertical distance from the interface. Consequently, local steadiness may be presumed, as, in fact, experimentally occurs.

For this initial model the absence of binder melts will be assumed. The limits of validity will then be determined by comparison of the model and experimental results. For the AP deflagration process the Guirao-Williams model⁽¹¹⁾ is accepted with an equilibrium assumption for the gas-solid (or viscous liquid) AP interface. Some minor modifications are introduced into this model for computational convenience; these will be described below. Use of this model will restrict the sandwich theory validity to the pressure

range 20-100 atm, because there is no AP theory capable of an explanation of observed phenomena above 100 atm and the low pressure deflagration limit of AP occurs near 20 atm.

Other usual assumptions are made to simplify the analysis which, while they lead to numerical error of order unity, do not alter significantly the scaling rules developed with respect to other variables. These assumptions are: a) the thermal and transport processes of the solid AP and binder are identical, b) the thermal and transport properties of all gas phase species are identical, c) the Lewis number is everywhere unity in the gas phase, d) the deflagration process takes place at constant pressure, e) heat conduction and mass transfer take place by temperature and concentration gradients, only, respectively, and the transport coefficients are independent of temperature in both the solid and gas phases. A final major assumption is that on any vertical line parallel to the binder-oxidizer interface the ρv product (density times velocity) is that as determined in the solid phase and all lateral velocities are zero (strictly true in the solid phase). This is in the spirit of the Burke-Schumann approximation as expounded in Reference (2). This does yield error in convection effects upon heat transfer, but exact treatment of the problem appears too complex at the present time.

The configuration is shown in Figure 1, in which the coordinate system is rendered stationary by a translation of the interface in the y direction at the rate r . Under the stated assumptions the equations for solution and the boundary conditions are:

Gas Phase Species Continuity

$$\lambda_g^* \left(\frac{\partial^2 Y_F^*}{\partial x^{*2}} + \frac{\partial^2 Y_F^*}{\partial y^{*2}} \right) = \rho^* v^* \frac{\partial Y_F^*}{\partial y^*} - w_F^* \quad (1)$$

$$\frac{\lambda_g^*}{c_p^*} \left(\frac{\partial^2 Y_B}{\partial x^{*2}} + \frac{\partial^2 Y_B}{\partial y^{*2}} \right) = \rho^* v^* \frac{\partial Y_B}{\partial y} \quad (2)$$

Rate Law

$$w_F^* = -k^* Y_F^{*2} e^{-E_g^*/R^* T^*} \quad (3)$$

Gas Phase Heat Transfer

$$\lambda_g^* \left(\frac{\partial^2 T^*}{\partial x^{*2}} + \frac{\partial^2 T^*}{\partial y^{*2}} \right) = \rho^* v^* c_p^* \frac{\partial T^*}{\partial y^*} + 2q_R^* w_F^* \quad (4)$$

Solid Phase Heat Transfer

$$\lambda_g^* \left(\frac{\partial^2 T^*}{\partial x^{*2}} + \frac{\partial^2 T^*}{\partial y^{*2}} \right) = \rho^* v^* c_s^* \frac{\partial T^*}{\partial y^*} \quad (5)$$

Boundary Conditions

$$\begin{aligned} Y_F(x, \infty) &= 0 & Y_F(-\infty, y) &= \bar{Y}_F(y) \\ T^*(x, -\infty) &= T_O^* & T^*(-\infty, y) &= \bar{T}^*(y) \\ T^*(\infty, y) &= T_O^* & T^*(x, \infty) &= T_O^* \end{aligned} \quad (6)$$

$$r_{n_B}^* = \bar{r}^* \cdot \bar{n}^* \Big|_B = b_B^* e^{-E_s^*/R^* T_s^*} \quad (7)$$

$$\lambda_g^* \frac{\partial T^*}{\partial n^*} \Big|_{s+} = \rho_s^* r_n^* q_s^* + \lambda_g^* \frac{\partial T^*}{\partial n^*} \Big|_{s-} \quad (8)$$

$$\rho^* D^* \frac{\partial Y_F}{\partial n^*} \Big|_{s+, AP} = -\rho_s^* r_n^* \left(\frac{1}{2} - Y_{F_s} \right) \quad (9)$$

$$\rho^* D^* \frac{\partial Y_B}{\partial n^*} \Big|_{s+, AP} = \rho_s^* r_n^* Y_{B_s} \quad (10)$$

$$p_{F_s}^* = b_F^* e^{-E_{sF}^*/RT_s^*} \quad (11)$$

$$T^* \text{ continuous, } \nabla T^* \text{ continuous within a phase} \quad (12)$$

The products of AP gasification are assumed NH_3 and HClO_4 which are assumed identical molecules for mass transfer computation. k^* is a rate coefficient for the assumed second order reaction; as written in Equation (3) k^* is not a fundamental preexponential constant but already has molecular constants and a factor p^{*2} absorbed into it. The factor 2 in front of $q_{R_F}^*$ in Equation (4) occurs because q_R^* will be quoted per unit mass of AP rather than per unit mass NH_3 . The equilibrium interface on AP is specified through Equation (10). The formulation, as far as the AP deflagration process is concerned, differs from that of Reference (11) in the following respects: a) no dilution of the NH_3 and HClO_4 is assumed at the solid-gas interface, although it is tacitly accounted for by the choice of a number for q_S^* ; b) calculations are simplified by taking the molecular weight of all species to be the same. The constants k^* and b_F^* will be so chosen to recover the same burn rate and surface temperature results as in Reference (10).

Equation (7) is the pyrolysis law for the binder, Equation (8) is the energy conservation law at the solid-gas interface, and Equations (9) and (10) are the interface diffusion laws. Note in Equation (8) that q_S^* undergoes a discontinuity at the binder-oxidizer interface and Equations (9) and (10) are only valid on the AP side of the interface. Shown in Table 1 are typical values used in this work for the various parameters.

Table 1
Numerical Values for Various Parameters

Quantity	Value	Reference
T_O^*	300 °K	Assumed
ρ_s^*	1.95 gm/cm ³	11
c_p^*	.3 cal/gm°K	11
c_s^*	.3 cal/gm°K	11
q_R^*	173 cal/gm	[to yield flame] temperature of 1205°K of Ref. (11)]
q_{SAP}^*	-100 cal/gm	11
λ_g^*	10^{-4} cal/cm sec°K	11
λ_s^*	9×10^{-4} cal/cm sec°K	11
E_g^*	15 kcal/mole	11
E_s^*	30 kcal/mole	11
E_{sB}^*	8.7 - 17 kcal/mole	14
b_B^*	1 - 150 cm/sec	14
q_{sB}^*	160 - 1004 cal/gm	14

Mathematical Character of the Problem

Equations (1) - (5) define an elliptic problem in the sense that what happens at one point in the field affects every other point. Furthermore an eigenvalue appears, $\rho^* v^* = \rho_s^* r^*$.

If the binder is hard to decompose and it assumes a nearly vertical surface, it appears obvious that the picture becomes one of a (nearly) flat plate of binder over which hot AP gases are flowing. If the Reynolds number based on distance along the binder were large enough this would revert to a parabolic problem because $\partial/\partial x \gg \partial/\partial y$ would result. However,

exactly at the binder-oxidizer interface, the Reynolds number is zero. Since it is precisely this region that is of interest, the full elliptic problem must be solved. In order to gain an idea of magnitudes involved here the equations are nondimensionalized with respect to a distance scale r_s^*/r^* and temperature T_o^* . Heats of gasification are made dimensionless by $c_p^* T_o^*$ and activation energies by $R^* T_o^*$. In order to locate the condensed phase - gas phase interface at a constant position the y variable is replaced by $\eta = y - y_s(x)$. The resulting dimensionless equations and boundary conditions are

$$L[Y_F] = \tilde{k} Y_F^2 e^{-\epsilon/g}$$

$$L[Y_B] = 0$$

$$(\text{Gas}) \quad L[g] = -2q_R \tilde{k} Y_F^2 e^{-\epsilon/g}$$

$$(\text{Solid}) \quad L[g] = (1 - \xi) g.$$

$$L = \frac{\partial^2}{\partial x^2} + z^2 \frac{\partial^2}{\partial \eta^2} - 2y'_s \frac{\partial^2}{\partial \eta \partial x} - y''_s \frac{\partial}{\partial \eta} - \xi \frac{\partial}{\partial \eta}$$

$$Y_F(x, \infty) = 0 \quad Y_F(-\infty, y) = \bar{Y}_F(y)$$

$$g(x, -\infty) = 1 \quad g(-\infty, y) = \bar{g}(y)$$

$$g(\infty, y) = 1 \quad g(x, \infty) = 1$$

$$1/z_B = \tilde{b}_B e^{-\epsilon_{S_B}/g_s}$$

$$\partial g / \partial n|_{s+} = \xi [q_s/z + \eta \partial g / \partial n|_{s-}]$$

$$\partial Y_F / \partial n|_{s+_{AP}} = -\frac{\xi}{z} (\frac{1}{2} - Y_{F_s})$$

$$\partial Y_B / \partial n|_{s+_{AP}} = \xi \frac{Y_{B_s}}{z}$$

$$Y_{F_s} = \tilde{b}_{F_s} e^{-\epsilon_{sF}/\epsilon_s}$$

g continuous, ∇g continuous within a phase (13)

Since y' and y_s'' are unknowns, the nonlinear character in Equations (13) is apparent. Nonlinearities also arise from the chemical reaction terms. The dimension α_s^*/r^* is known to be the "thickness" of the thermal wave which would occur in a planar regression. It is the reference dimension here. The parameter ξ in Equations (12) is nothing more than the ratio of a characteristic solid phase dimension (α_s^*/r^*) to the characteristic gas phase dimension (α_g^*/v^*). If there were no modification due to the reaction rate term, the gas phase distance over which significant heat transfer would occur would be of the order of α_g^*/v^* . Using the parameters of Table 1, $\xi = 9.0$, showing that the gas and solid phase characteristic scales are quite different. Furthermore, constructing the Reynolds number based upon y , it is found that $Re_y = \xi y$, so that when y is of the order of $1/\xi$ a transition is taking place between "low" and "high" Reynolds numbers. If important field quantity variations are taking place only over a gas phase distance of the order of $1/\xi$, the problem must be treated as elliptic with no simplifications possible through a boundary layer assumption. However, a rather simple method of solution will emerge if at some point in the flow field the boundary layer approximation may be involved. The use of this approximation will be illustrated below.

Solution by an Integral Technique

Pure AP Deflagration

Far from the binder the AP must undergo a planar deflagration but the angle θ is unknown; it is the eigenvalue of the problem. All

x-derivatives must vanish and Equations (13) become nonlinear ordinary differential equations in η along with the appropriate boundary conditions. The equation for the solid phase heat transfer may be solved exactly. The solution is

$$\bar{g} - 1 = (\bar{g}_s - 1) e^{\eta/z^2} \quad (14)$$

An overall energy balance yields the adiabatic flame temperature

$$\bar{g}_f = \bar{g}_s + q_R - q_s - \tilde{\eta}(\bar{g}_s - 1) \quad (15)$$

A first integral of the gas phase heat and mass transfer equations, subject to the boundary conditions, is

$$\bar{a}(\eta) \equiv \bar{g}(\eta) + 2q_R \bar{Y}_F(\eta) = \bar{g}_f = \bar{g}_s + 2q_R \bar{Y}_{F_s} \quad (16)$$

The solution is completed by assuming a functional form for $\bar{g}(\eta)$ as

$$\begin{aligned} \bar{g}(\eta) - \bar{g}_s &= (\bar{g}_f - \bar{g}_s) \frac{\eta}{\bar{c}} & \eta < \bar{c} \\ \bar{g}(\eta) &= \bar{g}_f & \eta \geq \bar{c} \end{aligned} \quad (17)$$

where \bar{c} is the η position where $\bar{Y}_F(\eta)$ vanishes, i.e. reaction is complete.

Now integrating the gas phase energy equation between $\eta = 0$ and $\eta = \bar{c}$ using the assumed form for $\bar{g}(\eta)$ from Equation (16), using the solid-gas interface boundary conditions and the equilibrium condition from Equations (12), the solution for the AP deflagration is completed as

$$\bar{c} = \frac{Y_{F_s} z^2}{5(\frac{1}{2} - \bar{Y}_{F_s})}$$

$$\begin{aligned}
 Q(\bar{c}) &= \tilde{k} \tilde{Y}_{F_s}^2 \bar{c} \int_0^1 \left(1 - \frac{\eta}{\bar{c}}\right)^2 e^{-\epsilon \sqrt{\bar{g}_s + (\bar{g}_f - \bar{g}_s) \frac{\eta}{\bar{c}}}} d\left(\frac{\eta}{\bar{c}}\right) \\
 &= Y_{F_s} \left(\frac{z^2}{\bar{c}} + \xi\right) = \xi/2 \\
 \tilde{Y}_{F_s} &= \tilde{b}_{F_s} e^{-\epsilon_{s_F} / \bar{g}_s}
 \end{aligned} \tag{18}$$

An extremely important point to note from Eqs. (18) is that they imply that the regression rate normal to the gas-solid interface is independent of $\bar{\theta}$, the inclination to the horizontal. For note, $Q(\bar{c})$ is an invariant. For a fixed \bar{g}_s , \tilde{Y}_{F_s} is fixed and $\bar{c} \propto z^2$. Therefore, $Q \propto \tilde{k} \tilde{Y}_{F_s}^2 \bar{c} \propto \tilde{k} z^2$. But $\tilde{k} \propto 1/r^2$ so that $r \propto z$ and $r_n = r \cos \theta = r/z$ is an invariant. Consequently, for any sandwich vertical regression rate, r , which is the eigenvalue of the problem, the AP far from the binder will regress normal to its surface at a fixed, unique value. The pertinent values for AP combustion are consequently only presented for $\bar{\theta} = 0$. To numerically complete the solution the following procedure is used. a) \bar{g}_s as a function of pressure is taken from Reference (11); b) Equation (14) yields \bar{g}_f (which is actually constant here because $\tilde{\eta} = 1$ and q_R and q_s are assumed independent of pressure); c) Equation (16) determines \tilde{Y}_{F_s} ; d) Equations (17) determine \bar{c} , \tilde{b}_{F_s} and \tilde{k} .

From the nondimensionalization procedure it may be recalled that $\tilde{k} \propto p^2/\bar{r}^2$. Therefore, if the rate, \bar{r} , is known at one pressure, it is known as a function of pressure. Shown in Table 2 are complete calculations for two sample pressures.

In Table 2 it will be noted that b_{F_s} is not quite constant. This is due to the use of a slightly higher E_{s_F} than in Reference (10). Furthermore,

\tilde{k} is not quite proportional to $(p/\bar{r})^2$. This is due to the fact that \bar{r} in Table 2 is the experimental value and it is known that between the two values of pressure of Table 2 the theory of Reference (11) slightly overestimates the pressure sensitivity of the deflagration rate. These details are not considered important for the current theory because a precise model for AP deflagration is not sought; only the deviations from a planar regression, due to the binder presence, are required and the above theory appears adequate to serve as a baseline for perturbations due to the binder.

Table 2

One Dimensional AP Deflagration Results

p	\bar{r}	α_s/r	\bar{T}_s	\bar{g}_s	\bar{Y}_{F_s}	\bar{g}_f	\bar{c}	b_F	\tilde{k}
(atm)	(cm/sec)	(μm)	($^{\circ}\text{K}$)					(atm)	
54.4	.735	20.9	880	2.93	.285	4.022	.1471	4.38×10^8	2.62×10^6
100.0	1.000	15.3	911	3.04	.258	4.022	.1183	4.06×10^8	3.39×10^6

Perturbed Solution

It is noted that there is only a very weak variation of the dimensionless parameters with pressure in Table 2 (because \bar{g}_s variations are weak with pressure) and therefore Eqs. (13) are nearly pressure invariant. Consequently, all further work will be carried out for the conditions that $\bar{g}_s = 2.93$ corresponding to $p = 54.4 \text{ atm.} = 800 \text{ psia.}$

Upon extensive investigation of the partial differential equations for small deviations from the one-dimensional regression it was determined that a) the deviations from the planar case in the gas phase could be expected to be simple deviations from the planar solution, but b) the solid phase deviations may be complex. By "simple" it is meant that the deviation is not oscillatory. Thus, if $g(x,y) = \bar{g}(x) + G(x,y)$ where $G(x,y)$ is the deviation from the pure AP case, $G(x,y)$ may be expected to have

monotonic behavior in η between the two end values $G[x, y_F(x)]$. Therefore it was decided to attempt an integral solution where

$$\begin{aligned} Y_F &= Y_{F_s}(x) \left[1 - \frac{\eta}{c(x)} \right] & \eta < c \\ Y_B &= Y_{B_s} + (Y_{B_c} - Y_{B_s}) \frac{\eta}{c} & \eta < c \\ Y_F &= 0 & \eta > c \\ g - g_s(x) &= \left[g_1(x) - g_s(x) \right] \frac{\eta}{c(x)} & \eta < c \end{aligned} \quad (19)$$

are guessed forms of the solution for the gas phase.

If the Eqs. (19) are placed in Eqs. (13) and integrated from $\eta = 0$ to $c(x)$ the result is three nonlinear ordinary differential equations in the unknowns Y_F , Y_{B_s} , Y_{B_c} , c , g_1 , g_s , y'_s and the η derivatives of g and Y_B at $\eta = c$. These derivatives appear because no functional form is specified for $\eta > c$. It is anticipated that these derivatives will be very small beyond the reaction region and one possible assumption is that they are zero. An alternate assumption has been employed and is discussed below. The diffusion boundary conditions and the equilibrium interface boundary condition provide three more relations for the nine unknowns. At $\eta = c$ which is of the order of magnitude of $1/\xi$, the Reynolds number is making a transition from low to high values, and it appears at this point reasonable to assume that $\frac{\partial}{\partial x} \gg \frac{\partial}{\partial y} = \frac{\partial}{\partial \eta}$. Making this assumption in Eqs. (13) there results

$$\begin{aligned} \left(\frac{\partial g}{\partial \eta} \right)_{\eta=c} &= \frac{1}{\xi} \left(\frac{\partial^2 g}{\partial x^2} \right)_{\eta=c} = \frac{1}{\xi} \frac{d^2 g_1}{dx^2} \\ \left(\frac{\partial Y_B}{\partial \eta} \right)_{\eta=c} &= \frac{1}{\xi} \left(\frac{\partial^2 Y_B}{\partial x^2} \right)_{\eta=c} = \frac{1}{\xi} \frac{d^2 Y_{B_c}}{dx^2} \end{aligned} \quad (20)$$

Eqs. (20) eliminate two of the above unknowns and one further relation is needed. For algebraic simplicity another differential equation is obtained by taking an η - moment of the equation

$$L[a] = 0 \quad a = g + 2q_R Y_{F_s}$$

derivable from Eqs. (13), and integrating from 0 to c.

In order for a numerical integration to proceed smoothly to $x = -\infty$ an asymptotic solution is desirable. Consequently, a solution was first sought which is a small perturbation about the planar AP deflagration state. Letting

$$Y_{F_s} = \bar{Y}_{F_s} + Y_{F_s}(x)$$

$$g_1 = \bar{g}_1 + G_1(x)$$

$$g_s = \bar{g}_s + G_s(x)$$

$$c = \bar{c} + C(x)$$

$$y_s = Y(x),$$

$$Y_{B_s} = Y_{B_s}(x)$$

$$Y_{B_c} = Y_{B_c}(x)$$

substituting these forms into the nonlinear ordinary differential equations and boundary conditions, making use of the AP solution properties, and neglecting products and squares of perturbation quantities, there results the following linearized set of equations and boundary conditions

$$\frac{1}{2}[\bar{Y}_{F_s} C'' + \bar{c} Y_{F_s}''] + Y'' \bar{Y}_{F_s} + \bar{Y}_{F_s}' Y_{F_s}' = Q_{g_1} G + Q_{Y_{F_s}} Y_{F_s} + Q_c C + Q_{g_s} G_s \quad (21)$$

$$\frac{1}{2}[\bar{c} G_1'' + \bar{c} G_s'' + C''(\bar{g}_s - \bar{g}_1)] + \frac{z^2}{\bar{c}} G_1'' = (G_1 - G_s) \left(\frac{z^2}{\bar{c}} + \xi \right) + 2\bar{Y}_{F_s}' (G_1' - G_s')$$

$$- \left(\frac{-2Y_{F_s}'}{\bar{c}} + \frac{\bar{c}^2}{\bar{c}^2} \right) (\bar{g}_1 - \bar{g}_s) + Y''(\bar{g}_1 - \bar{g}_s) - 2q_R(Q_{Y_{F_s}} Y_{F_s} + Q_{g_1} G_1 + Q_c C$$

$$+ Q_{g_s} G_s) \quad (22)$$

$$\frac{1}{2} \bar{c} (\gamma_{B_c}'' + \gamma_{B_s}'') + \frac{\bar{z}^2 \gamma_B''}{\bar{c}} = (\bar{c} + \frac{\bar{z}^2}{\bar{c}}) (\gamma_{B_c} - \gamma_{B_s}) + 2\bar{y}_s' (\gamma_{B_c}' - \gamma_{B_s}') \quad (23)$$

$$(\gamma_{B_c} - \gamma_{B_s}) \frac{\bar{z}^2}{\bar{c}} - \bar{y}_s' \gamma_{B_s}' = \bar{c} \gamma_{B_s} \quad (24)$$

$$\bar{y}_s' \gamma_{F_s}' = -\bar{c} \gamma_{F_s} + \frac{\bar{z}^2 \bar{c} \gamma_{F_s}}{\bar{c}^2} - 2\bar{y}_s' \bar{y}_{F_s}' - \frac{\bar{z}^2}{\bar{c}} \gamma_{F_s} \quad (25)$$

$$\gamma_{F_s} = \frac{\bar{y}_{F_s} E_{F_s}}{\bar{c}^2} G_s \quad (26)$$

$$G_1(-\infty) = G_s(-\infty) :: \gamma_{F_s}(-\infty) = \gamma_{B_c}(-\infty) = \gamma_{B_s}(-\infty) = Y'(-\infty) = C(-\infty) = 0 \quad (27)$$

Here Q_{g_1} , Q_{g_c} , Q_{g_s} and $Q_{Y_{F_s}}$ are partial derivatives of the reaction rate integral which may be numerically evaluated. Note that Eqs. (23) and (24) are decoupled from the rest of the system. Because Eqs. (21)-(27) are linear and homogeneous, they possess solutions like, say, $G_1 = A G_1 e^{mx}$. Since $2Y_F + Y_B + Y_P = 1$, the binder equations must also have solutions $\gamma_{B_c} = A_{\gamma_{B_c}} e^{mx}$ where the m is the same. So there are two sets of equations which may be investigated. Since the equations are homogeneous, the determinant of the coefficient matrix must equal zero for a solution to exist. From Eqs. (21), (22), and (25) $m = m_1(\bar{\theta})$ is therefore developed. From Eqs. (24) and (25) $m = m_2(\bar{\theta})$ is developed and the results are shown on Fig. 2. Only real values of m were numerically investigated because the only unique solutions which will properly attach to the binder are for real m , as will be seen later. It is seen that there is a unique $\bar{\theta}$ for

$$m = 6.4 \quad \bar{\theta} = 2^\circ$$

That is, an eigenvalue exists. The AP assumes a nearly horizontal surface far from the binder so that the burn rate is only slightly higher

and the physical properties of the binder. A question now to be asked is whether or not this linear solution may be used instead of a full nonlinear solution for binders of practical interest. The usual physical expectation is that a linearized theory will be reasonable if the perturbation quantities remain within some prescribed fraction of the corresponding baseline quantity. Viewing Fig. 3 and focusing on g_1 , for example, if an arbitrary limit of validity is set that $(g_1 - \bar{g}_1)/\bar{g}_1 < 10\%$, it appears that the solution might be expected to be valid for $x < 0.6$. Adopting this criterion, a procedure to match to the binder is required for the linearized solution.

Location of the Binder

It will be noticed that the above solution is independent of the solid phase solution. In fact the heat transfer condition of Eqs. (13) and the surface temperature of the gas phase solution form boundary conditions for the solid phase heat transfer. Since the attempt here is to work with the asymptotic solution to a linear set of equations, the consistent linearized solid phase equation from Eqs. (13) is for $g = \bar{g}(\eta) + G(x, \eta)$

$$\frac{\partial^2 G}{\partial x^2} + \frac{\partial^2 G}{\partial \eta^2} - \frac{\partial G}{\partial \eta} = Y' \frac{\partial \bar{g}}{\partial \eta} \quad (28)$$

where the simplifying assumption of $\bar{y}_s' = 0$ has been made in accordance with the above gas phase solution. Letting $G = \hat{g} + Y \frac{\partial \bar{g}}{\partial \eta}$, Eq. (27) becomes

$$\frac{\partial^2 \hat{g}}{\partial \eta^2} + \frac{\partial^2 \hat{g}}{\partial x^2} - \frac{\partial \hat{g}}{\partial \eta} = 0$$

which has the solution

$$\begin{aligned} \hat{g} &= e^{\eta/2} e^{m_g x} [G_0 \cos m_g \eta + G_1 \sin m_g \eta] \\ m_g &= (m^2 - \frac{1}{4})^{\frac{1}{2}} \end{aligned} \quad (29)$$

This solution has a feature that

$$G_s = G_o e^{mx} + Y \frac{\partial \bar{g}}{\partial \eta} \quad (7)$$

which determines G_o from the gas phase solution. A most important feature of the solution is the creation of an oscillatory ripple of very short wavelength (of order $1/m_g \approx 1/m$) superimposed on the monotonically varying temperature of the undisturbed solution. What happens, therefore, is that in both the solid phase and gas phase the distance scales over which rapid transitions are made are now of the same order of magnitude (of order $1/\xi$). In a sense, the short distance scale of the gas phase is imposed upon the solid phase.

To complete the solid phase solution Eq. (28) is substituted into the interface heat transfer condition of Eqs. (13) and G_1 is determined. Now at any x position in the eigensolution to the AP problem the heat transfer vector in the gas and solid phases is known. Since this must be a continuous quantity and the temperature is a continuous quantity, but q_s undergoes a discontinuity, there must be a surface slope discontinuity at the binder. In the interface energy conservation relation of Equations (13) the solid and gas phase heat transfer vectors may be computed from the AP solution and this equation becomes a relation for the binder heat of gasification as a function of its surface slope. The result is

$$q_{s_B} = m G_s y'_B \left(\frac{\xi - 1}{\xi} \right) + (1 + y'_B y'_s) \left\{ \frac{g_1 - g_s}{\xi c} - (g_s - 1) (1 + Y) - \frac{G_o}{2} - m_g G_1 \right\} \quad (30)$$

The pyrolysis condition of Equations (13) gives an additional relation between the surface slope and the binder properties

$$\frac{1}{z_B} = \tilde{b}_B e^{-\epsilon_{s_B}/g_s} \quad (31)$$

At any x position, then, Equations (29 and 30) together with the AP eigensolution define an allowable binder attachment and a functional equation

$$b_B = b_B(\epsilon_{s_B}, q_{s_B}; x)$$

$$y'_B = y_B(\epsilon_{s_B}, q_{s_B}; x)$$

For the case of $p = 54.4$ atm these results are shown in Figures 4 and 5 for two values of ϵ_{s_B} which correspond closely to HTPB and CTPB binders.⁽¹⁴⁾ Also, knowing q_s and b_B for HTPB and CTPB⁽¹⁴⁾ the actual point at which these two binders would attach is shown on Figures 4 and 5.* There are several points worthy of note. First, for these binders, the x position of compatibility with the AP solution occurs where very little change from a flat AP surface has taken place. Consequently, the linear AP eigensolution can be used with confidence as a good approximation to the solution of the nonlinear problem. Polyurethane, shown on Fig. 4 would also attach to a nearly flat AP surface. A check of the fluorocarbon binder data of Ref. (14) also shows an attachment at negative x . The second important point is that the binder slope is very nearly vertical at the attachment point. This is the primary information desired, in addition to the AP surface profile, so no attempt is made to continue the solution to the right of the attachment point to find the binder profile. The third major point, referring back to Fig. 3, is that the solid phase heat

* The activation energies for HTPB and CTPB do not exactly fit the numbers of Figs. 4 and 5. What has been done is to compute a b_B to fit the known binder pyrolysis data at a temperature g_s , assuming the activation energies of the figures.

transfer vector points from the binder toward the AP. This indicates that at least for a short distance above the interface the binder temperature must be increasing, probably due to the fact that the highest temperature AP gases are at positive η .

DISCUSSION OF RESULTS

A solution has been obtained for the shape of the deflagrating AP surface when it is adjacent to an inert dry binder. The eigenvalue, the vertical regression rate, has been found to be independent of binder type and to deviate only very slightly from the pure AP burn rate, as has been experimentally observed. Except for selected binders there would be very little visible effect of the binder upon the surface shape and the result is virtually independent of pressure. The distance scale over which a visible transition would take place from planar AP to the binder is of the order of microns. The current theory assumes a dry binder; it is known, however, that binder melt flows exist for all binders tested heretofore in the sandwich configuration and that these melt flows run several hundred microns onto the AP surface. Furthermore, surface roughness dimensions of the order of microns develop during deflagrations. Consequently, few of the predicted phenomena are capable of being observed. A theory including the effects of melt flows is necessary.

The theory predicts, however, that if the melts do not occur there should be a sharp discontinuity in slope at the binder-oxidizer interface. This has recently been seen for catalyzed sandwiches⁽¹⁵⁾ for which the melt extent is markedly reduced (for unknown reasons). Although the current theory is not directly applicable to catalyzed situations the interface conditions responsible for the slope discontinuity are applicable. It appears that melt flows dominate the development of the

surface shape if melts occur.

The current theory shows that the heat flow vector near the gas-solid interface and AP-binder solid interface is from the binder toward the AP in the solid phase. Consequently, there must exist a weak (hot) portion of the binder slightly up from the four-corner interface and into the binder. This might account for the appearance of "notches" in the binder sometimes seen in quenched samples.^(1,2,4,15) The violence of the quenching process may eject the part of the binder which is weaker than surrounding parts.

The current analysis shows a very weak dependence of surface shape upon pressure. This independence has been observed experimentally, but the comparison between theory and experiment cannot be made precisely because binder melts have occurred in all the experiments.

If the AP particle size is sufficiently large the current analysis may form the basis for a deflagration theory of a heterogeneous propellant, if the binder were dry. The largest natural dimension which occurs in this theory is the thermal wave depth which is of the order of $20 \mu\text{m}$ at 800 psia. Consequently, for AP particle sizes larger than this dimension there may be some merit in applying this technique to a real propellant. An extension to the case of a finite binder thickness would be required, however, unless AP particle sizes substantially in excess of the thermal wave depth were considered because the typical binder widths would be less than the typical thermal depth in the binder. Such an extension is not deemed difficult to attain.

REFERENCES

1. Hightower, J. D. and Price, E. W., "Experimental Studies Relating to the Combustion Mechanism of Composite Propellants," Astronautica Acta, 14, (1968), 11-21.
2. Varney, A. M., "Experimental Investigation of the Burning Mechanism of Ammonium Perchlorate Composite Propellants, Ph.D. Dissertation, Georgia Institute of Technology, (1971).
3. Jones, H. E., "An Experimental Investigation Relating to the Combustion Mechanism of Ammonium Perchlorate Composite Propellants," Ph.D. Dissertation, Georgia Institute of Technology, (1971).
4. Boggs, T. L. and Zurn, T. E., "The Deflagration of Ammonium Perchlorate-Polymeric Binder Sandwich Models," Combustion Science and Technology, 4, (1972), 279-292.
5. Boggs, T. L., Zurn, D. E., Strahle, W. C., Handley, J. C., and Milkie, T. T., "Mechanisms of Combustion," NWC TP 5514, July 1973.
6. Nadaud, L., "Models Used at ONERA to Interpret Combustion Phenomena in Heterogeneous Solid Propellants," Combustion and Flame, 12, (1968), 177-195.
7. Austin, T. D., "Flame Temperature Profile of Ammonium Perchlorate Fuel Binder Sandwiches," 4th ICRPG Combustion Conference, CPIA Publication No. 162, Vol. 1, (1967).
8. Brown, W. E., Kennedy, J. R., and Netzer, D. W., "A Study of AP/PBAA Sandwich and AP Pellet Combustion," 9th JANNAF Combustion Meeting, CPIA Publication 231, Vol. II, (1972).
9. Bakhman, N. and Librovich, V. B., "Flame Propagation Along Solid Fuel-Solid Oxidizer Interface," Combustion and Flame, 15, (1970), 143-155.
10. Nachbar, W., "A Theoretical Study of the Burning of a Solid Propellant Sandwich," Solid Propellant Rocket Research, Academic Press, New York, 1960.
11. Guirao, C. and Williams, F. A., "A Model for Ammonium Perchlorate Deflagration between 20 and 100 atm," AIAA Journal, 9, (1971), 1345-1356.
12. Williams, F. A., Combustion Theory, Addison-Wesley, Reading (1965), p. 39.
13. Strahle, W. C., "Solid Propellant Sandwich Deflagration Analysis, AIAA Paper No. 74-123, 1974.
14. Cohen, N. S., Fleming, R. W., and Derr, R. L., "Role of Binder in Solid Propellant Combustion," AIAA Paper No. 72-1121, (1972).

15. Handley, J. C. and Strahle, W. C., "The Behavior of Several Catalysts in the Combustion of Solid Propellant Sandwiches," AIAA Paper No. 74-122, 1974.

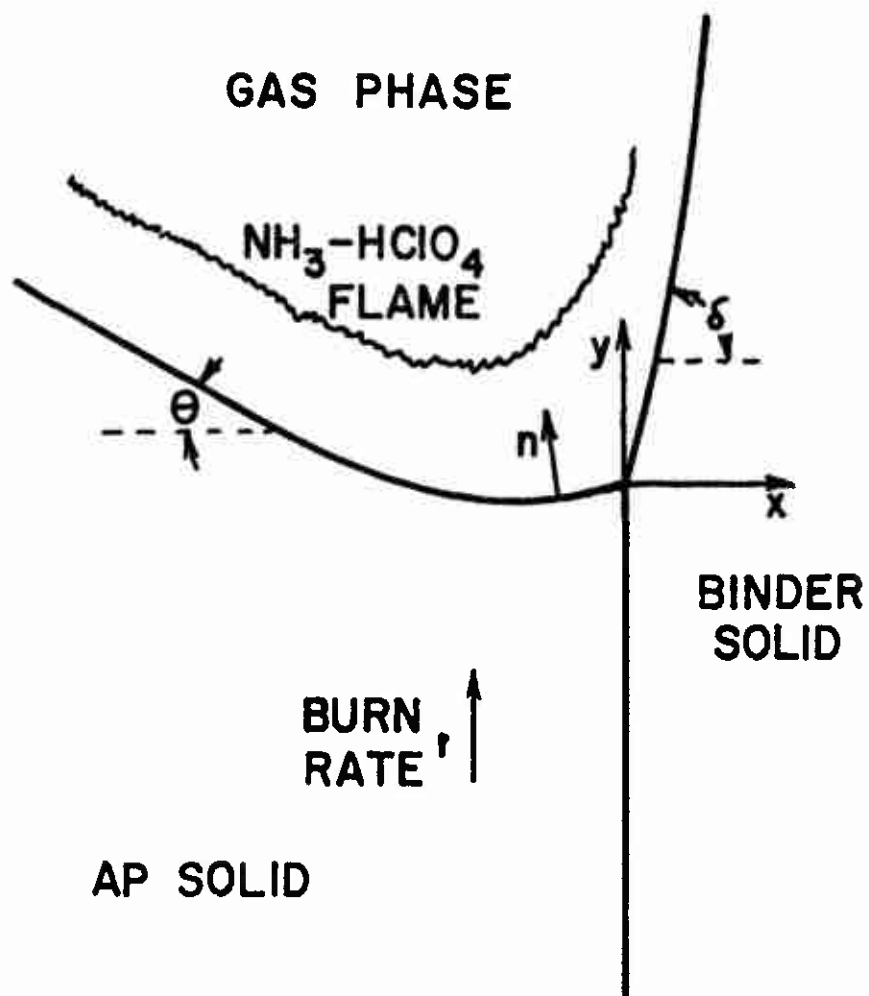


Figure 1. Sandwich Schematic and the Coordinate System

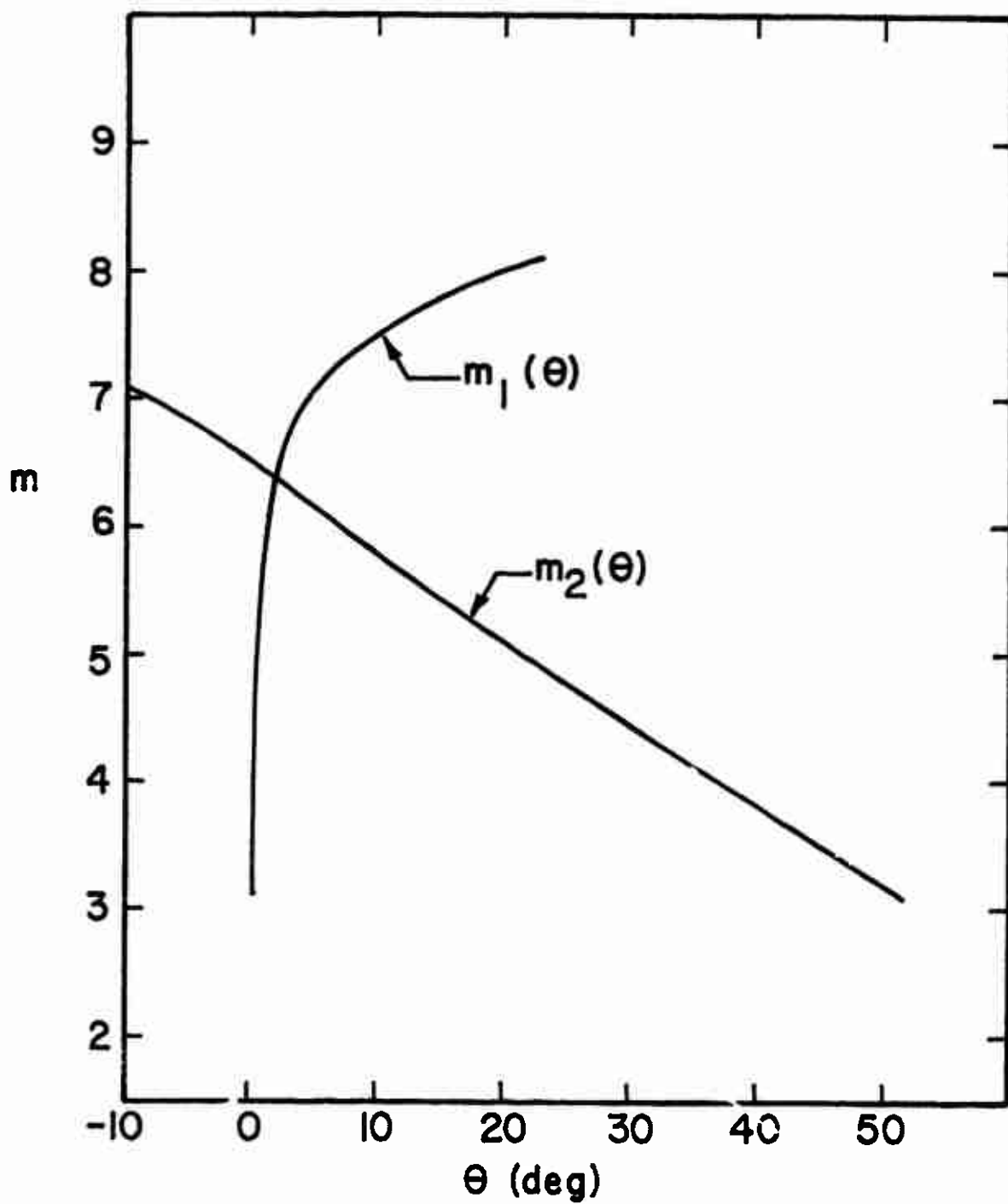


Figure 2. Roots of the Linearized Sets of Equations

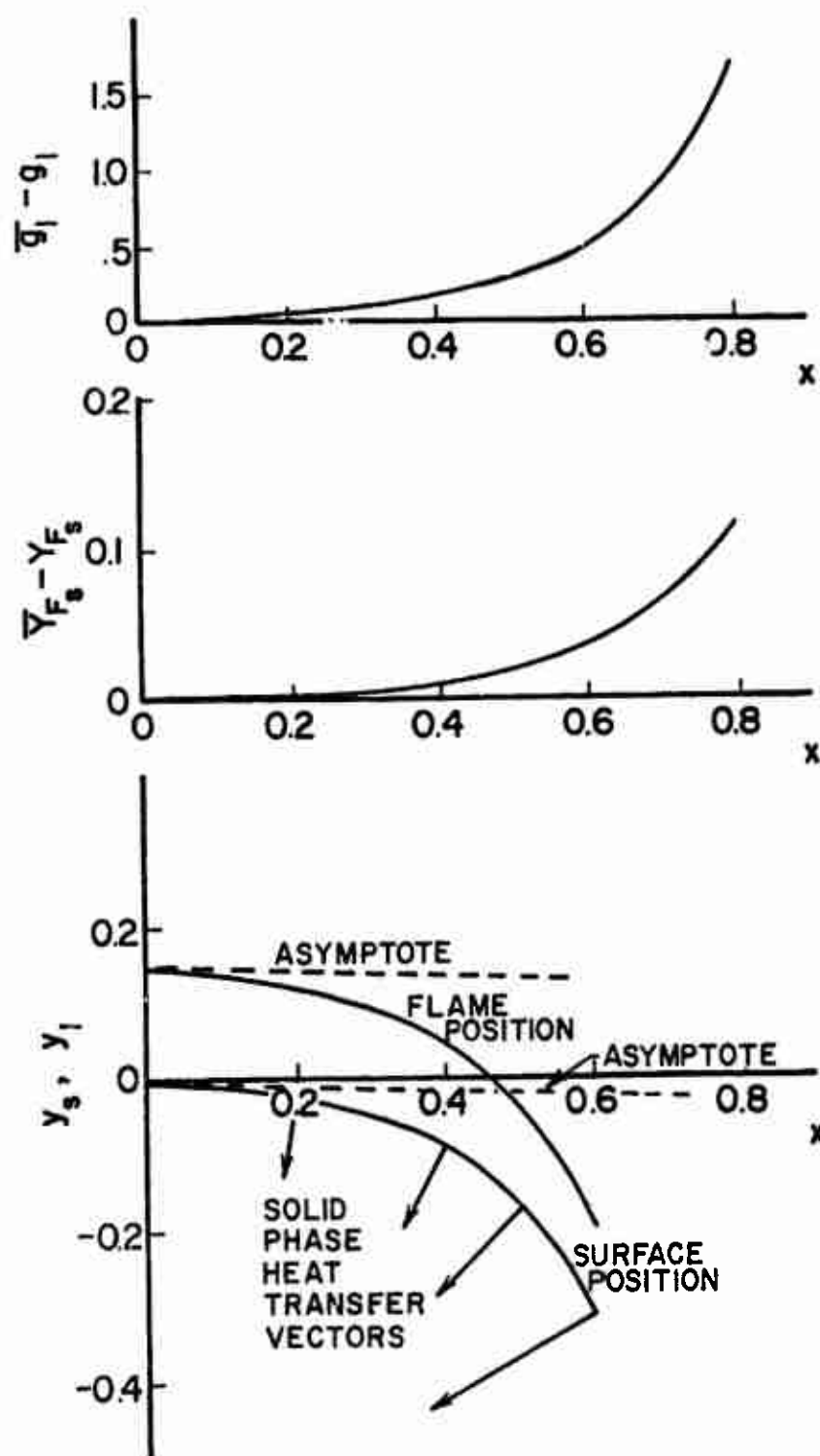


Figure 3. Surface, Flame Standoff, Surface NH_3 Mass Fraction, Flame Temperature and Solid Phase Heat Transfer Vector Profiles

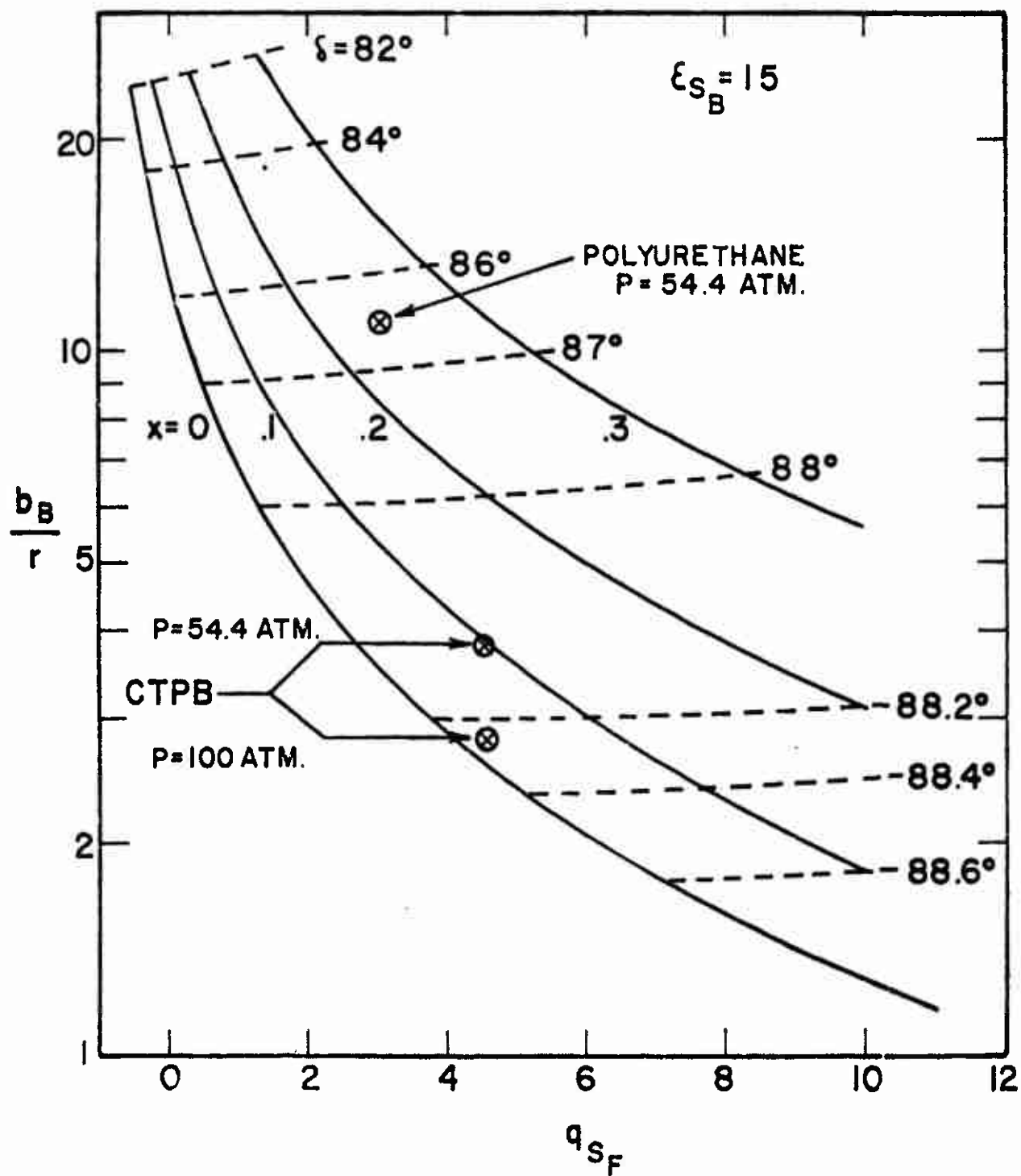


Figure 4. Binder Properties for Attachment to the AP Solution, $\epsilon_{SB} = 15$

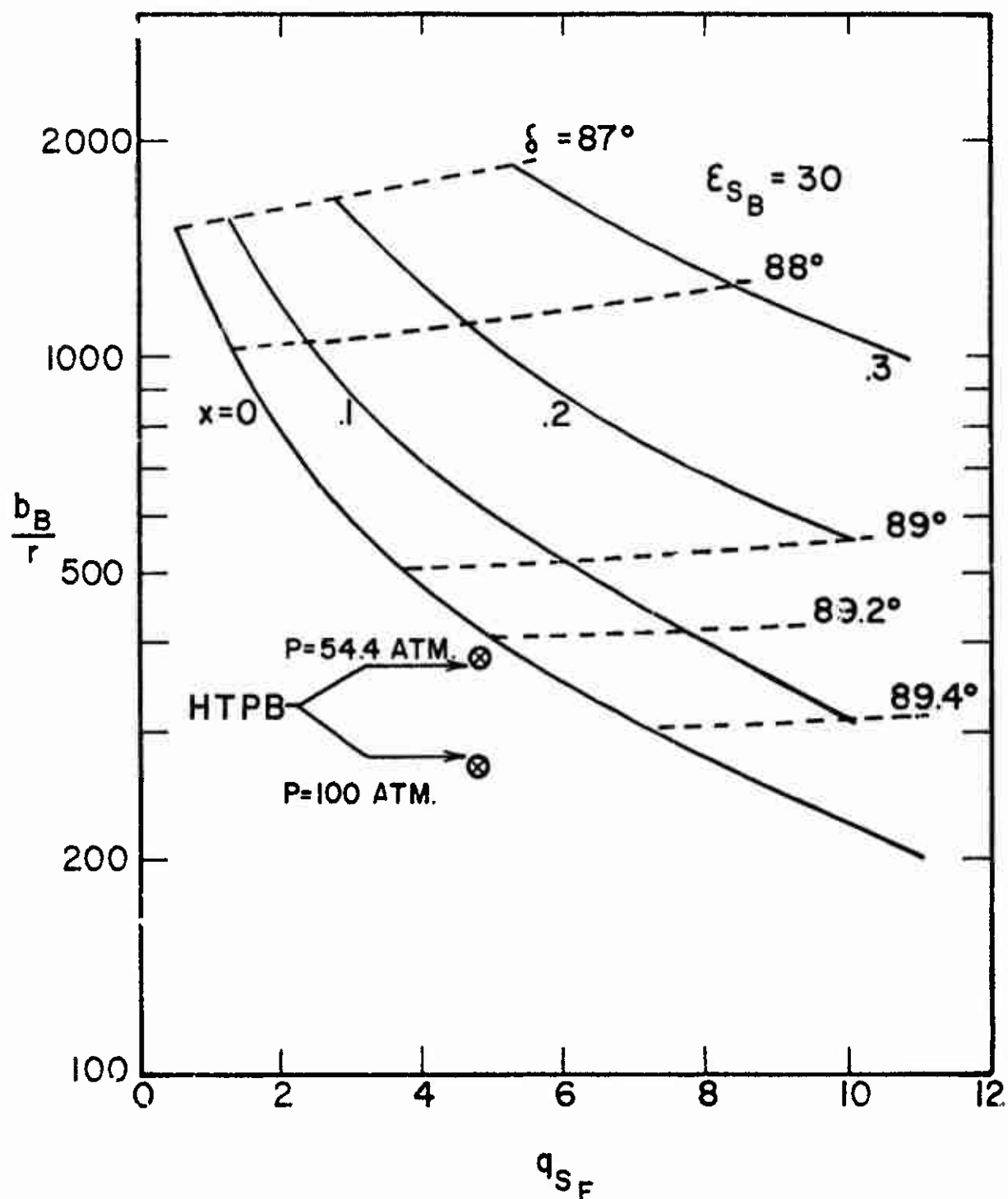


Figure 5. Binder Properties for Attachment to the AP Solution, $\epsilon_{s_B} = 30$